THEORETICAL INVESTIGATION OF METAMATERIALS: SRR STRUCTURES AND PERIODIC ARRAYS OF THIN CONDUCTING WIRES

A THESIS SUBMITTED TO
THE GRADUATE SCHOOL OF NATURAL AND APPLIED SCIENCES
OF
MIDDLE EAST TECHNICAL UNIVERSITY

BY

KAZIM OZAN ATEŞ

IN PARTIAL FULLFILLMENT OF THE REQUIREMENTS
FOR
THE DEGREE OF MASTER OF SCIENCE
IN
ELECTRICAL AND ELECTRONICS ENGINEERING

MAY 2008

Approval of the thesis:

THEORETICAL INVESTIGATION OF METAMATERIALS: SRR STRUCTURES AND PERIODIC ARRAYS OF THIN CONDUCTING WIRES

submitted by **K. OZAN ATEŞ** in partial fulfillment of the requirements for the degree of **Master of Science in Electrical and Electronics Engineering Department, Middle East Technical University** by,

Prof. Dr. Canan Özgen
Dean, Graduate School of **Natural and Applied Sciences** _____

Prof. Dr. İsmet Erkmen
Head of Department, **Electrical and Electronics Engineering** _____

Prof. Dr. Gönül Turhan Sayan
Supervisor, **Electrical and Electronics Engineering Dept., METU** _____

Examining Committee Members:

Prof. Dr. Mustafa Kuzuoğlu
Electrical and Electronics Engineering Dept., METU _____

Prof. Dr. Gönül Turhan Sayan
Electrical and Electronics Engineering Dept., METU _____

Prof. Dr. Kemal Leblebicioğlu
Electrical and Electronics Engineering Dept., METU _____

Prof. Dr. Gülbin Dural
Electrical and Electronics Engineering Dept., METU _____

İlksen Acunalp, (MSc)
Int. Crypt. and Elect. Resc. Ins., Ankara _____

Date: May 5, 2008

I hereby declare that all information in this document has been obtained and presented in accordance with academic rules and ethical conduct. I also declare that, as required by these rules and conduct, I have fully cited and referenced all material and results that are not original to this work.

Name, Last name : K. OZAN ATEŞ

Signature :

ABSTRACT

THEORETICAL INVESTIGATION OF METAMATERIALS: SRR STRUCTURES AND PERIODIC ARRAYS OF THIN CONDUCTING WIRES

Ateş, K. Ozan

M.Sc., Department of Electrical and Electronics Engineering
Supervisor: Prof. Dr. Gönül Turhan Sayan

May 2008, 70 pages

In recent years, there has been an increasing interest on left handed metamaterials because of their possible innovative applications. The pioneer study introducing such materials was brought out by V. G. Veselago in 1968 [1]. In his work, Veselago proposed a medium having simultaneously negative electric permittivity and magnetic permeability and investigated its electromagnetic characteristics. He found out that the electric field, magnetic field and the propagation vector form a left handed triplet, thus named such materials as "Left Handed Materials". Despite the significance of Veselago's inferences, the metamaterial theory stayed dormant for nearly 30 years. Towards the end of 1990s, the physically realizable left handed materials were built as the combination of two periodical structures; Split Ring Resonators (SRRs) and metallic thin wire arrays [4-5].

In this thesis, electrical and magnetic characteristics of the left handed metamaterials are theoretically investigated by using the analytical models for their permittivity and permeability functions with respect to frequency. For this purpose, first, two basic metamaterial structures; the Split Ring Resonators and Thin Metallic Wire Arrays are studied individually and their electrical and magnetic characteristics are examined. Finally, the composite left handed structure containing both SRRs and thin wires is studied to investigate the resulting simultaneous resonance properties and to estimate their overall effective permeability and permittivity functions.

Keywords: Metamaterials, Left Handed Metamaterials, Negative Permittivity, Negative Permeability, Split Ring Resonators, Metallic Wire Arrays, Composite Left Handed Metamaterials.

ÖZ

METAMALZEMELERİN TEORİK İNCELEMESİ: SRR YAPILARI VE İNCE İLETKEN TELLERDEN OLUŞAN PERİYODİK DİZİNLER

Ateş, K. Ozan

Yüksek Lisans, Elektrik ve Elektronik Mühendisliği Bölümü

Tez Danışmanı: Prof. Dr. Gönül Turhan Sayan

Mayıs 2008, 70 sayfa

Son yıllarda, olası yenilikçi uygulamalarından dolayı solak metamalzemelere ilgi giderek artmıştır. Bu malzemeler üzerine ilk çalışma 1968 yılında V. G. Veselago tarafından yapılmıştır [1]. Veselago bu çalışmasında elektrik geçirgenlik ve manyetik geçirgenliğin aynı anda negatif olabileceği bir ortam öne sürmüş ve bu ortamın elektromanyetik özelliklerini incelemiştir. Ayrıca, bu materyallerin elektrik alan, manyetik alan ve propagasyon vektörlerinin solak bir üçleme oluşturduğunu da keşfetmiş, bu nedenle böyle malzemeleri "Solak Malzemeler" olarak adlandırmıştır. Veselago'nun çıkarımlarının önemine rağmen, metamalzeme teorisi üzerinde yaklaşık 30 yıl kadar başka bir çalışma yapılmamıştır. 1990'ların sonlarına

doğru, solak metamalzemeler iki farklı periyodik yapı olan Yarık Halka Rezonatörleri ve metalik ince tel dizinlerinin birleştirilmesiyle fiziksel olarak oluşturulmuştur [4-5].

Bu tezde, elektrik ve manyetik geçirgenlik fonksiyonlarının frekansa bağımlı analitik modellerinin oluşturulması yoluyla solak metamalzemelerin elektrik ve manyetik karakteristiklerinin kuramsal olarak incelenmesi gerçekleştirilmiştir. Bu amaç doğrultusunda, iki temel metamalzeme yapı olan Yarık Halka Rezonatörleri ve Metalik Tel Dizinleri önce ayrı ayrı değerlendirilmiş ve bu yapıların elektrik ve manyetik özellikleri incelenmiştir. Son olarak, yarık halka rezonatörleri ve metalik tel dizinlerinin oluşturduğu birleşik solak yapıyla elde edilen tınlaşım özellikleri incelenmiş ve ortaya çıkan efektif elektrik ve manyetik geçirgenlik fonksiyonlarının kestirimi gerçekleştirilmiştir.

Anahtar Sözcükler: Metamalzemeler, Solak Metamalzemeler, Negatif Elektrik Geçirgenlik, Negatif Manyetik Geçirgenlik, Yarık Halka Rezonatörleri, Metal Tel Dizinleri, Birleşik Solak Metamalzemeler.

To Alpcan and Yeliz...

ACKNOWLEDGEMENTS

I would like to thank with my deepest gratitude and appreciation to my supervisor Prof. Dr. Gönül Turhan Sayan for her guidance, valuable suggestions and great patience.

I would like to thank to my colleagues for their assistance and patience. And of course to my recent company ASELSAN and Mr. Caner Şeker for his large perspective, guidance and support at all level of my business life.

I would like to thank to my friends who have tolerated my absence during this thesis process and still did not give up being my friend. And of course to İlksen, who has even participated to my thesis examining committee.

I would like to thank to my family, my little brother Alpcan for his unique love. I am quite sure that I would not be able to achieve any of these without his shine on my life. I am sincerely longing for his endless existence throughout the rest of my life. Can, you are the one.

And finally I would like to thank to Yeliz for her love, motivating encouragement, invaluable support and unique gorgeousness. “Morse-coding signals; they pulsate and wake me up!”

TABLE OF CONTENTS

ABSTRACT iv

ÖZ vi

ACKNOWLEDGMENTS ix

TABLE OF CONTENTS x

LIST OF FIGURES xii

CHAPTERS

1. INTRODUCTION 1

2. OBTAINING NEGATIVE PERMEABILITY 6

3. OBTAINING NEGATIVE PERMITTIVITY 30

4. COMPOSITE METAMATERIAL POSSESSING NEGATIVE PERMITTIVITY AND PERMEABILITY 44

5. PARAMETERS AFFECTING THE RESONANCE BEHAVIOR OF METAMATERIALS 50

5.1 Changing the Resonance Behavior of the SRR Elements 51

5.1.1. Effect of Split Width 52

5.1.2. Effect of Gap Distance 55

5.1.3. Effect of Ring Width 55

5.1.4. Effect of Additional Capacitance 58

5.1.5. Effect of Substrate Permittivity 60

5.2 Changing the Resonance Behavior of the Wire Structure 60

5.2.1. Effect of Wire Radius 62

5.2.2. Effect of Lattice Distance 63

6. CONCLUSION 65

REFERENCES 68

LIST OF FIGURES

Figure 1-1 Positioning of field and propagation vectors for left handed metamaterials……...2

Figure 1-2 Presentation of a typical SRR element 4

Figure 2-1 Square array of metallic cylinders as in Pendry's study [4]……...7

Figure 2-2 Unit cell presentation of the structure with the lattice constant *a* 8

Figure 2-3 Cylindrical element having an internal capacitive structure called split ring where *d* is the separation of two rings [4]……..10

Figure 2-4 The effective permeability simulation for the Split Ring Sheets 12

Figure 2-5 SRR particle geometry as examined in [7]……....13

Figure 2-6 Capacitive parameters and charge presentation of a SRR [7] 15

Figure 2-7 Orientation of a SRR particle in the reference coordinate system ... 17

Figure 2-8 The simulation results for real (solid) and the imaginary (dashed) parts of the averaged magnetic polarizability of a random SRR.....23

Figure 2-9 The simulation results for real (solid) and the imaginary (dashed) parts of the averaged electric polarizability of a random SRR..... 24

Figure 2-10 Effective permittivity simulation results for a random SRR. Real (solid) and the imaginary (dashed) parts are presented …….....26

Figure 2-11 Effective permeability simulation results for a random SRR. Real (solid) and the imaginary (dashed) parts are presented 27

Figure 2-12 The cubic cell presentation suggested for the derivation of effective medium parameters [7] 27

Figure 2-13 Effective permittivity simulation results for the proposed cubic cell. The real (solid) and the imaginary (dashed) parts are presented.....28

Figure 2-14 Effective permeability simulation results for the proposed cubic cell. The real (solid) and the imaginary (dashed) parts are presented.....29

Figure 3-1 An array of wires aligned as a square lattice [2] 32

Figure 3-2 Simulation of the permittivity for an aluminum wire array; real (solid) and imaginary (dashed) parts are presented. 36

Figure 3-3 Numerical simulations of the band structure for aluminum wire array where real (top) and imaginary (bottom) parts of κ (a) are shown...37

Figure 3-4 Inductor Array equivalent of the thin wire array [8] 38

Figure 3-5 Wire array vertically standing between opposing metal plates (top) and relevant parameter presentations (bottom) [8].....40

Figure 3-6 Equivalent unit circuit of the thin wire array [8].....41

Figure 3-7 Numerical simulations of the band structure for aluminum wire array, real (solid) and imaginary (dashed) parts of the wave vector are presented.....43

Figure 4-1 Real parts of electric permittivity (solid) and magnetic permeability (dashed) of the denoted cubic SRR structure 45

Figure 4-2 Effective permittivity of the aluminum wire array; real (solid) and imaginary (dashed) parts are presented 46

Figure 4-3 Composite SRR and Wire Element Structure 47

Figure 4-4 The real parts of effective permittivity functions of thin wire array (solid) and SRR cubic structure (dashed) 48

Figure 4-5 The real parts of effective permeability functions of thin wire array (solid) and SRR cubic structure (dashed) 49

Figure 5-1 SRR element orientation in the structure suggested in [15] 52

Figure 5-2 Figure 5-2: Real part of the magnetic permeability of the SRR array for different values of the split widths. Split widths are taken as 0.2 mm (solid), 0.3 mm (dashed), 0.4 mm (dot) and 0.5 mm (dashed-dot)……..54

Figure 5-3 Variation in resonance frequency of SRR array due to changing only split width 54

Figure 5-4 Real part of the magnetic permeability of SRR elements for different values of the gap distance. Gap distances are taken as 0.2 mm (solid), 0.3 mm (dashed), 0.4 mm (dot) and 0.5 mm (dashed-dot).....56

Figure 5-5 Variation in resonant frequency of SRRs due to changing gap distance……..56

Figure 5-6 Real part of the magnetic permeability of SRR elements for different values of the ring widths. Ring widths are taken as 0.9 mm (solid), 0.7 mm (dashed), 0.5 mm (dot)…….57

Figure 5-7 Variation in resonant frequency of SRRs due to changing ring width……..58

Figure 5-8 Real part of the magnetic permeability of SRR array for different values of the additional capacitance across the outer ring split. Capacitance values are taken as 0.1 pf (solid), 0.2 pf (dashed), 0.5 pf (dot) and 0.8 pf (dashed-dot)…….59

Figure 5-9 Real part of the magnetic permeability of SRR array for different values of the substrate relative permittivity. The permittivities are taken as 3.85 (solid), 2.85 (dashed), 1.85 (dot)…….61

Figure 5-10 Real part of electric permittivity of the wire array for different values of the wire radius. The radii are taken as 0.5 μm (solid), 1.0 μm (dashed), 1.5 μm (dot) and 2.0 μm (dash-dot)……...63

Figure 5-11 Real part of the effective permittivity of the wire array for different values of the lattice distance. The lattice distances are taken as 3 mm (solid), 4 mm (dashed), 5 mm (dot)……...64

CHAPTER 1

INTRODUCTION

Materials having some unusual properties which are not observed in nature are called as metamaterials. The main academic interest on metamaterial theory is the realization of periodic structures possessing simultaneously negative permittivity and permeability characteristics. Permittivity and permeability parameters are known to take positive values for naturally occurring materials and they determine the electric and the magnetic behavior of the associated medium. Throughout this thesis, metamaterial structures with negative permittivity and negative permeability parameters over certain frequency bands are going to be investigated.

In 1968, V. G. Veselago studied a hypothetical medium possessing simultaneously negative permittivity and permeability for the first time [1] and theoretically investigated how the main electromagnetic properties of that medium are affected. He found out that when the signs of permittivity and permeability are both changed to negative; the refractive index changed sign, the phenomena of Doppler Effect and the Čerenkov Radiation were reversed and then, the medium can support backward waves. Moreover, the electric field vector $\boldsymbol{E}$, magnetic field vector $\boldsymbol{H}$ and the propagation vector $\boldsymbol{k}$ were observed to form a left hended vector triplet in an orientation as shown in Fig.1-1. Relevantly, such a medium is named as “Left Handed Metamaterial” [1].

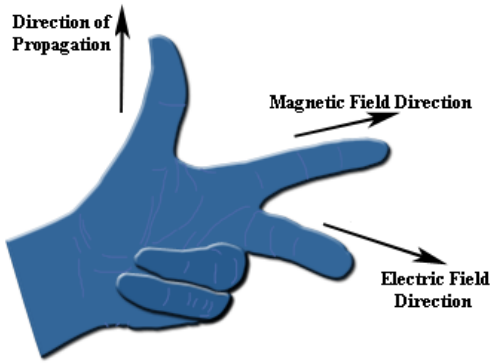

Figure 1-1: Positioning of field and propagation vectors for left handed metamaterials

Veselago pointed out in [1] that, an electromagnetic wave propagates in a medium if and only if the medium parameters have the same sign, i.e. no propagation will be expected in a medium if permittivity and permeability of that medium are in different signs. In view of that fact, a left handed metamaterial should posses negative permittivity and permeability over a common frequency band simultaneously. However in nature, there is no known material possessing this kind of double negative parameter behavior.

Veselago's innovative inferences could not attract significant academic attention for nearly 30 years. In the mid-90s, together with the technological and academic developments, it became possible to experimentally demonstrate left handed metamaterials and this opportunity caused the theory to gain a renovated interest [2-5, 18].

In fact, the negative permittivity was already a known property of plasma medium below the plasma frequency even in late 1950s [19]. In view of that fact, in 1996, J. B. Pendy studied the metallic wire array which was known to simulate the plasma medium [6]. Unfortunately, there was a limitation about the plasma operating frequency that the well established plasmon oscillation would have been seen only

around the plasma frequency which was around the near UV or the visible region for naturally occurring plasma. Far below the plasma frequency, dissipation destroyed all traces of plasmon thus J. B. Pendry's primary concern became to reduce the plasma frequency towards the microwave band. In this sense, Pendry worked on the metallic wire array and found out that sufficiently thin metallic wires were capable to yield negative permittivity characteristics at microwave frequencies as well as maintaining the plasmon behavior [2].

Later, Harbin Institute of Technology in China studied on Pendry's results and they developed an analytical model for the permittivity formula of the wire array by making use of the Transmission Line Theory [8]. The Chinese group first built a transmission line equivalent circuit for the wire array where the wires no longer have the restriction to align in a square symmetry, i.e. the spacing between the wires along the two different axes would be altered without violating the overall periodicity. Their permittivity model gave the same results when the wires are arranged in square symmetric alignment so their results were coherent with Pendry's.

On the other hand, obtaining negative permeability was a more complicated issue compared to the negative permittivity case since there was no known naturally occurring material to be inspired from. In that context, J. B. Pendry was motivated to search for the ways of developing an artificial medium displaying negative permeability characteristics in 1999 [4]. For that purpose he started to work on the metallic cylinder array which was already known to simulate the plasma medium. In order to enhance the magnetic response of this structure, he imposed some capacitive elements over each metallic cylinder in the array. Additional capacitive elements increased the nonlinearity as well as the magnetic response in the array. Consequently he observed that a capacitive array of sheets wound on the cylinders would be capable of creating negative permeability property [4]. He named these capacitive elements as Split Ring Resonators (SRRs) and further studies also proved

the negative permeability capability of this structure [5, 18, 20-23]. A SRR is composed of basically two concentric rings with splits in the opposite sides as presented in Fig. 1-2. Extensive studies about the SRRs have indicated that they are capable to exhibit magneto electric coupling i.e. either external electric or magnetic field constitutes both electric and magnetic dipoles [7]. However the electrical resonances of the SRR elements have been observed to be very poor compared to the magnetic resonances. Furthermore, the negative permittivity and negative permeability resonance bands do not overlap [7, 15, 20, 22, and 23].

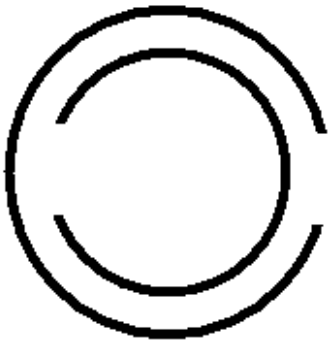

Figure 1-2: Presentation of a typical SRR element

In other words, neither an array of thin wires nor an array of SRR elements solely is capable of providing simultaneous negative permittivity and negative permeability. Therefore, these two structures are combined in a way that the composition would be able to exhibit negative permittivity and permeability characteristic concurrently by overlapping the negative permittivity band of the wire array and the negative permeability band of the SRR array [5].

In this thesis, first, the negative permeability phenomenon is studied through the SRR elements. For that purpose, previously derived [7] analytical formulas of the permeability and the permittivity functions of a periodic SRR structure are studied

and then computed by Matlab codes written in this thesis work. Next, the negative permittivity issue is examined for a metallic wire array. The analytical models of the relevant permittivity and permeability parameters are again investigated and simulated. Then, the overall left handed metamaterial model is studied via combining the SRRs and the thin wire array. In this, composite left handed metamaterial structure, the possibility of modifying the value of resonance frequency is examined. Effects of various structural parameters of the SRR such as the split spacing, loop radii, spacing between the loops and substrate are investigated in determining the resonance frequency of the metamaterial. Then, the parameters affecting the permittivity characteristics of the wire array are studied as changing the wire radius and lattice distance. It is seen that there is a great flexibility in adjusting the negative permittivity resonance band since the wire array exhibits a broader range of negative permittivity region compared to the negative permeability region of the SRR array.

The organization of the remaining part of this thesis will be as follows: Chapter 2 will present the theory behind the simulation of negative permeability in metamaterials. Theoretical investigation of metamaterials with negative permittivity will be given in Chapter 3. Composite metamaterials having both negative permeability and negative permittivity are discussed in Chapter 4. Effects of structural parameters on the resonance frequency of the composite metamaterials are investigated in Chapter 5. Finally, the thesis is concluded in Chapter 6 with relevant discussions of the results.

CHAPTER 2

OBTAINING NEGATIVE PERMEABILITY

There exists no known material possessing negative permeability characteristics. Relevantly in the metamaterial literature, some novel artificial structures are to be developed in order to obtain such a behavior. The Split Ring Resonator (SRR) is the most frequently discussed of these structures. In this chapter negative permeability issue is going to be studied using the SRR structure. In doing so, the analytical models of the SRR are going to be examined.

The pioneer studies in the metamaterial literature focused on the periodical array structures. The most significant of them was J. B. Pendry's study about metallic cylindrical array in 1999 [4]. It was already a known fact even in those days that plasma medium could be simulated by periodic metallic cylinders [6]. In his study, Pendry was motivated to modify this plasma medium in order to yield negative permeability characteristic. In fact, plasma medium was known to be nearly nonmagnetic however Pendry claimed that by increasing the capacitive effect in the structure, the magnetic response of a medium could be enhanced. He imposed some nonmagnetic conducting sheets through each cylinder of the array in order to enhance the capacitive impedance of the structure. Consequently, he observed that the permeability function would be able to take negative values for such an array. In the preceding section, the studies of Pendry are going to be investigated and his results are going to be simulated by Matlab codes.

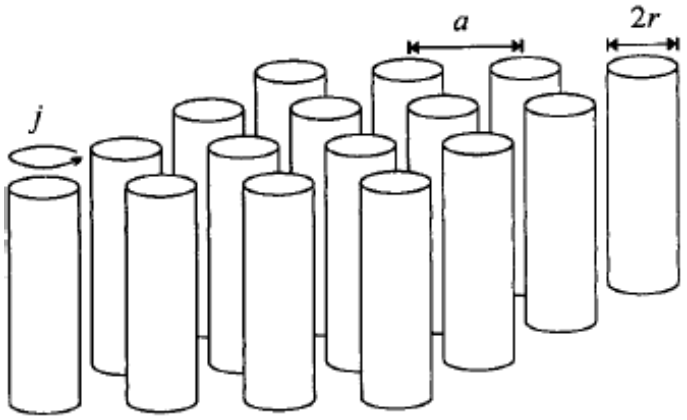

Figure 2-1: Square array of metallic cylinders as in Pendry's study [4]

The cylindrical array structure that Pendry discussed is demonstrated in Fig. 2-1. The cylinders are oriented in a square periodicity and a current per unit length *j* is assumed to be flowing around the surface of a single cylinder. Here, *a* is the lattice distance between the cylinders and *r* is the cylinder radius. Since effective medium parameters are going to be defined for this structure, the effective medium theory should be applicable. The mutual effects between the array elements will be negligible. If the lattice distance *a* and the wire radius *r* are chosen much smaller than the wavelength of any possible radiation [4]. Therefore, if the radiation occurs at a frequency of ω, the lattice distance and the frequency should satisfy the condition in (2.1) and then the cylinders may be assumed as wire elements. Relevantly, the averaged field presentations can be written as in (2.2).

$$a << \lambda = 2\pi C_0 \omega^{-1} \tag{2.1}$$

$$\boldsymbol{B}_{ave} = \mu_{eff}\, \mu_o \boldsymbol{H}_{ave}$$

$$\boldsymbol{D}_{ave} = \varepsilon_{eff} \varepsilon_o \boldsymbol{E}_{ave} \tag{2.2}$$

Consider now the Maxwell's equations in the integral form where the integration loop *c* encloses an area S.

$$\oint_c H.dl = +\frac{\partial}{\partial t}\int_S D \cdot dS$$

$$\oint_c E.dl = -\frac{\partial}{\partial t}\int_S B \cdot dS \qquad (2.3)$$

The wire array is assumed to be composed of square unit cells as presented in Fig 2-2 where each cell contains a single wire element. However, the effective medium theory restriction should still be considered that the lattice distance *a* and wire radius *r* must be much smaller than the wavelength of any possible radiation.

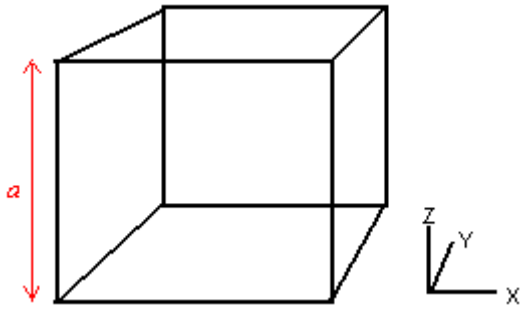

Figure 2-2: Unit cell presentation of the structure with the lattice constant *a*

The magnetic field intensity $\boldsymbol{H}_{ave}$ is averaged along each axis and the magnetic flux density $\boldsymbol{B}_{ave}$ is averaged over each faces of unit cubic cell as denoted in (2.4) and (2.5).

$$(H_{ave})_x = a^{-1}\int_{r=(0,0,0)}^{r=(a,0,0)} H \cdot dr$$

$$(H_{ave})_y = a^{-1}\int_{r=(0,0,0)}^{r=(0,a,0)} H \cdot dr$$

$$(H_{ave})_z = a^{-1}\int_{r=(0,0,0)}^{r=(0,0,a)} H \cdot dr \qquad (2.4)$$

$$(B_{ave})_x = a^{-2}\int_{S_x} B \cdot dS$$

$$(B_{ave})_y = a^{-2}\int_{S_y} B \cdot dS$$

$$(B_{ave})_z = a^{-2}\int_{S_z} B \cdot dS \tag{2.5}$$

S_x, S_y and S_z are the surfaces perpendicular to the unit vectors in the directions of x, y and z axes, respectively. Hence, the ratio of expressions (2.4) and (2.5) gives the permeability function for the cubic wire array structure:

$$(\mu_{\text{eff}})_{\text{x}} = (B_{\text{ave}})_{\text{x}} / (\mu_{\text{o}} H_{\text{ave}})_{\text{x}}$$

$$(\mu_{\text{eff}})_{\text{y}} = (B_{\text{ave}})_{\text{y}} / (\mu_{\text{o}} H_{\text{ave}})_{\text{y}}$$

$$(\mu_{\text{eff}})_{\text{z}} = (B_{\text{ave}})_{\text{z}} / (\mu_{\text{o}} H_{\text{ave}})_{\text{z}} \tag{2.6}$$

The effective permeability of the wire array is derived in [4] via calculating the averaged magnetic field intensity and relevant flux density throughout the unit cell as given in (2.6), yielding an effective permeability function as (2.7)

$$\mu_{eff} = 1 - \frac{\pi r^2}{a^2}\left[1 + i\frac{2\sigma}{\omega r \mu_0}\right]^{-1} \tag{2.7}$$

here σ is the resistance of the cylinder surface per unit area. If the wires are made up of a highly conductive material then the term including σ is high enough to dominate the denominator of (2.7) and the effective permeability turns out to be the compact form as in (2.8)

$$\mu_{eff} \approx 1 + i\frac{\pi r^3 \omega \mu_0}{2\sigma a^2} \qquad \text{and} \qquad \sigma >> \omega r \mu_0 \tag{2.8}$$

The permeability equation in (2.8) is quite significant that the wire array exhibits nearly no magnetic response. For the purpose of enhancing the magnetic characteristics, Pendry claimed that the capacitive effect should be improved throughout the structure [4]. For this purpose, capacitive sheet elements are imposed around each cylinder in the array. Then a typical element of the array turns out to be as shown in Fig. (2-3). Imposed capacitive elements are mainly two different sized concentric cylindrical sheets which have splits in the opposing sides. These elements are named as Split Ring Resonators and arose significant academic attention in the literature [4, 5, 20-23].

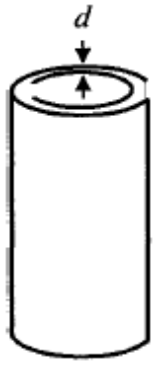

Figure 2-3: Cylindrical element having an internal capacitive structure called split ring where *d* is the separation of two rings [4].

Similar to the previous wire array, the permeability function of the periodic SRR structure is obtained by the ratio of the averaged magnetic field intensity and relevant flux density throughout the unit cell. Detailed calculations in [4] yield an effective permeability function for the split ring array as given in (2.9)

$$\mu_{eff} = 1 - \frac{\frac{\pi r^2}{a^2}}{1 + \frac{2\sigma j}{\omega r \mu_0} - \frac{3dC_0^{\ 2}}{\pi^2 \omega^2 r^3}} \tag{2.9}$$

The permeability function in (2.9) has zero value at a critical frequency. This frequency may also be named as a plasma frequency since the discussions are developed from a plasma medium model. The relevant plasma frequency for the capacitive cylinder array is then derived as in (2.10)

$$\omega_{mp} = \sqrt{\frac{3}{\pi^2 \mu_0 C r^3 (1-F)}} = \sqrt{\frac{3dC_0^{\ 2}}{\pi^2 r^3 (1-\frac{\pi r^2}{a^2})}} \qquad (2.10)$$

Permeability function derived for the capacitive cylinder array in (2-9) is simulated by a Matlab code and the results are presented in Fig. 2-4. During the simulation, the cylindrical sheets are chosen to be made up of a material having $\sigma \approx 0.01$. Element radius is taken as r = 2 mm, lattice constant is taken as a=5 mm and the separation of split rings are taken as d = 0.1 mm. Consequently, using (2.10), the relevant plasma frequency is calculated as $f_{mp} = (2\pi)^{-1}\ \omega_{mp}$ = 5.25 GHz. The results in Fig. 2-4 are quite important that by imposing some capacitive element through each wire, the permeability function would be able to possess a resonance region around 5.1 GHz. It is also worth to note that below the resonant frequency, μ_{eff} is significantly enhanced but above the resonance μ_{eff} is less than unity and may have negative values close to the resonance. The magnetic resonance behavior of the capacitive cylinders is mostly related to the capacitance between the sheets and magnetic inductance of each sheet pair [4].

The SRRs have attracted significant academic interest and numerous studies are devoted to the investigation and realization of these structures [4, 5, 20-23]. One of the most significant studies is brought out by Simovsky and Sauviac in 2004 [7]. They were motivated to derive a more complete analytical model for the permeability and permittivity parameters of the SRR element. In that way, effects of compensation of the electric dipole resonance and the separation of the magnetic and electric resonances over the frequency band are also taken into account. The two loops of an SRR particle were assumed to be two resonators which were

strongly coupled both via the common magnetic flux and via the mutual capacitance in between. Relevantly, the mutual coupling between the SRR loops was considered as a combination of inductive and capacitive couplings [7]. Fig 2-5 presents the SRR element geometry and its size parameters as proposed in [7]. In this figure, r_o is the wire radius, a_1, a_2 are the loop radii, d is the spacing between the two loops and δ is the split spacing of each loops.

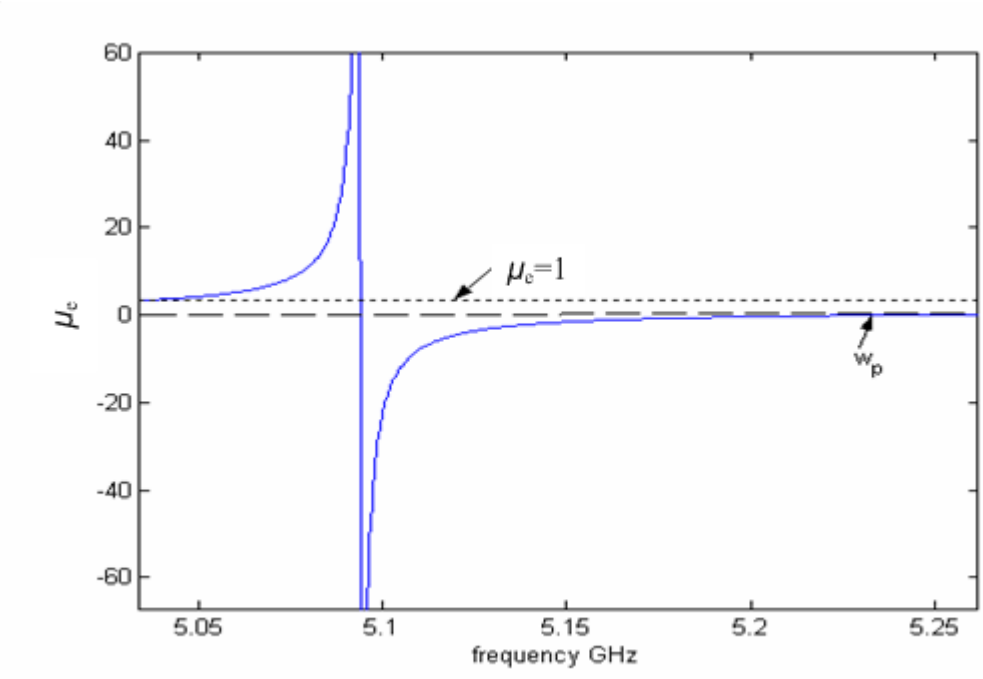

Figure 2-4: The effective permeability simulation for the Split Ring Sheets

Experimental results [5, 20-23] show that SRR elements are able to indicate magneto electric coupling, i.e. external electric fields induce both electric and magnetic dipoles in the particle, and similarly external magnetic fields also cause both electric and magnetic dipoles. This magneto electric interaction may be reduced by choosing opposite positioning of the splits of the two loops however the effects of the two loops do not cancel out since the loops are of different sizes. In

order to observe the magneto electric property of a SRR element, firstly the resonance behavior of its electric and magnetic polarizabilities is going to be investigated. Following polarizability calculations, the effective medium parameters of the SRR structure are going to be obtained by using standard Maxwell Garnett formulas.

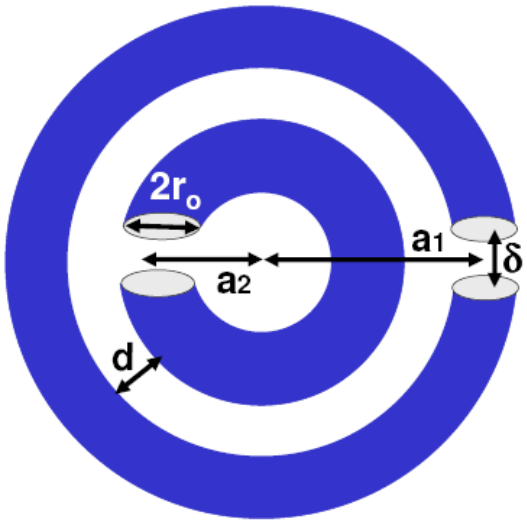

Figure 2-5: SRR particle geometry as examined in [7]

For the purpose of deriving the electric and magnetic polarizability parameters, the SRR element is assumed to be located a homogeneous dielectric medium of infinite extent with the permittivity ε. Then the electric and magnetic polarizabilities, a_e and a_m of one split ring element are dyadic coefficients relating the local electric and magnetic fields E_{loc}, H_{loc} with the induced electric and magnetic dipole moments [9].

$$p = \bar{\bar{a}}_{ee} \bullet E_{loc} + \bar{\bar{a}}_{em} \bullet H_{loc}$$

$$m = \bar{\bar{a}}_{me} \bullet E_{loc} + \bar{\bar{a}}_{mm} \bullet H_{loc} \qquad (2.11)$$

Here the electric and magnetic moments p and m of the SRR element can be considered as vector sums of the moments of the outer and inner loops, i.e. $p = p_1 + p_2$ and $m = m_1 + m_2$. As indicated by Lagarkov *et al*. [10], equations for the complex amplitudes of currents induced at the broken ends of both SRR rings can be written as in (2.12).

$$(Z_{C1} + Z_{L1})I_1 + Z_{12}I_2 = \varepsilon_{E1} + \varepsilon_{H1}$$

$$Z_{12}I_1 + (Z_{C2} + Z_{L2})I_2 = \varepsilon_{E2} + \varepsilon_{H2} \qquad (2.12)$$

where ε_E and ε_H are the electromotive forces generated by external electric and magnetic fields and the index 1 presents the outer ring while the index 2 presents the inner ring. The total capacitance is chosen to include the capacitive mutual coupling as well in order to simplify the overall mutual coupling term. Relevantly, two factors contribute to total loop capacitances C_1 and C_2; the first factor is due to the split of each loop and the second factor rises from the capacitive coupling between the loops. Fig 2-6 describes these two factors contributing to the loop capacitances where C_s presents the capacitive factor of the splits and C_{mut} presents the capacitive factor of the coupling in-between. The term Z_{12} is denoted as the mutual impedance of the loops ($Z_{12} = j\omega M$) where M is the mutual inductance between the two loops. Additionally, Z_{L1} and Z_{L2} present the inductive loop impedances ($Z_{L1}=j\omega L_1$, $Z_{L2} = j\omega L_2$) and relevantly Z_C is the capacitive loop impedance [$Z_{C1}=1/(j\omega C_1)$, $Z_{C2} = 1/(j\omega C_2)$]. Consequently, the loop impedances could be obtained as in (2.13).

$L = \mu_0 R(\log(\frac{8R}{r_0}) - 2)$ R=$a_{1,2}$ are the loop inductances

$M = \mu_0 a_1 \left[(1-\xi)\log(\frac{4}{\xi}) - 2 + \xi \right]$ is the mutual inductance

where $\xi = (a_1 - a_2)/2a_1$ is the space ratio

$C_1 = C_{S1} + \frac{C_{mut}}{2}$ $C_2 = C_{S2} + \frac{C_{mut}}{2}$ are loop total capacitances

$C_{mut} = \frac{2\pi\varepsilon\varepsilon_0 a}{\arccos h(\frac{d}{2r_0})}$ $C_s = \frac{\pi r_0 \varepsilon\varepsilon_0}{\delta}$ are mutual and self capacitances (2.13)

here a in the mutual capacitance term presents the averaged loop radius as $a = (a_1 + a_2)/2$.

The eigenfrequencies could be obtained by equating the determinant of (2.12) to zero. Then, in the balance condition, the electromotive forces $\mathcal{E}_E$ and $\mathcal{E}_H$ should vanish yielding the closed equation set of (2.14)

$$(Z_{C1} + Z_{L1})(Z_{C2} + Z_{L2}) - Z_{12}^2 = 0 \qquad (2.14)$$

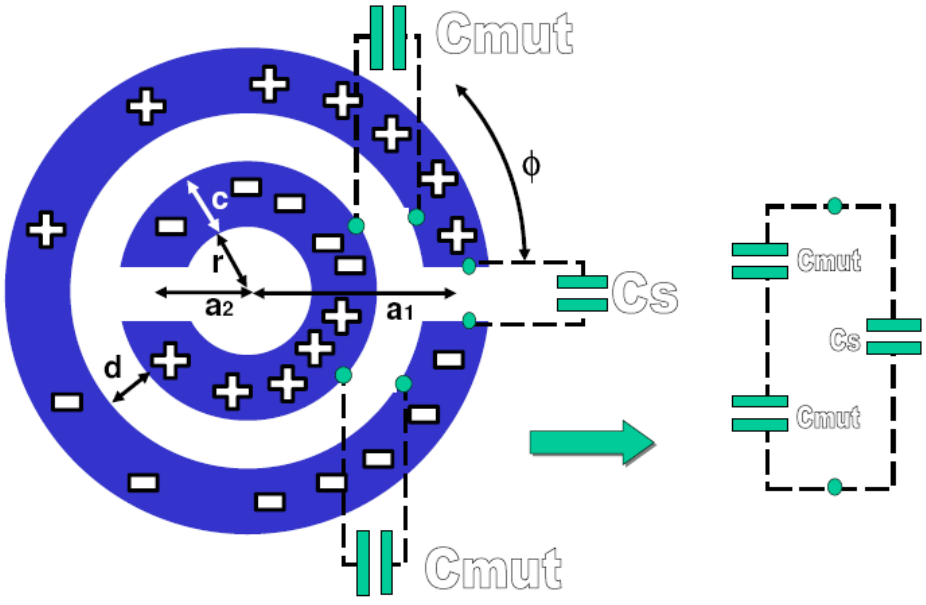

Figure 2-6: Capacitive parameters and charge presentation of a SRR [7]

Substituting the inductive, capacitive and mutual impedances into (2.14), it could be rewritten as in (2.15)

$$(\frac{1}{j\omega C_1} + j\omega L_1 + r_1)(\frac{1}{j\omega C_2} + j\omega L_2 + r_2) + \omega^2 M^2 = 0 \qquad (2.15)$$

where r_1 and r_2 are small resistances related to the radiation and Joule's losses in both loops. These losses lead to an additional imaginary correction term denoted as κ (ω) therefore, equation (2.15) may be written as in the form of (2.16). If each loop of the SRR is chosen to be made of a perfectly conducting material, then κ describes only radiation losses and its value may be calculated from the energy balance condition [12].

$$(\omega^2 - \omega_-^2)(\omega^2 - \omega_+^2) + j\kappa(\omega) = 0 \qquad (2.16)$$

Comparing (2.15) and (2.16) gives the relation between the two eigenfrequencies:

$$2(\frac{\omega_\pm}{\omega_m})^2 = \frac{\omega_m^2}{\omega_1^2} + \frac{\omega_m^2}{\omega_2^2} \pm \sqrt{(\frac{\omega_m^2}{\omega_1^2} + \frac{\omega_m^2}{\omega_2^2})^2 - 4} \qquad (2.17)$$

using the notations;

$$\omega_m{}^2 = \frac{1}{\sqrt{C_1 C_2 (L_1 L_2 - M^2)}}, \qquad \omega_{1,2}^2 = \frac{1}{C_{1,2} L_{1,2}}$$

The two resonance frequencies $\omega_\pm$ correspond to two eigenmodes presenting electric and magnetic resonances. If these frequencies differ drastically, two separate resonances will occur. However in practice $\omega_+ \approx \omega_-$ thus, two resonance bands overlap and a single resonance is observed. In the following parts, this event is going to be discussed.

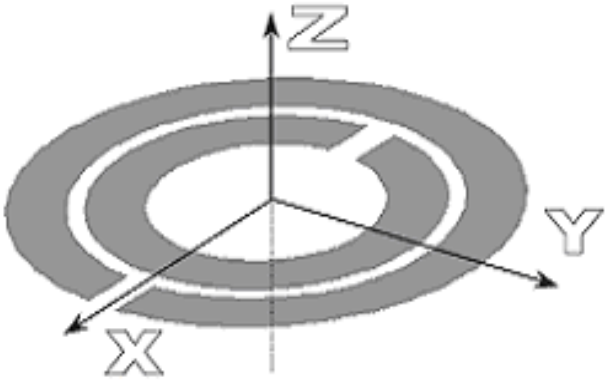

Figure 2-7: Orientation of a SRR particle in the reference coordinate system

Consider now a magnetic excitation with $\boldsymbol{E}_{loc}$= 0 and $\boldsymbol{H}_{loc} = z_o H_{loc}$. Then the only component of the magnetic moment is the one which is vertical to the SRR particle, i.e. $\bar{\bar{a}}_{mm} = z_0 z_0 a_{mm}^{zz}$. The detailed calculations yield a compact magnetic polarizability formula in the form given as in (2.18) [7]:

$$a_{mm}^{zz} = -D\omega^2 \frac{B_1(\omega^2 - \omega_1'^2) + B_2(\omega^2 - \omega_2'^2)}{\Delta + j\kappa} \tag{2.18}$$

The parameters used in (2.18) are defined as:

$$B_1 = S_1(S_1 L_2 - MS_2) \qquad B_2 = S_2(S_2 L_1 - MS_1)$$

$$S_{1,2} = \pi a_{1,2}^2 \qquad \Delta = (\omega^2 - \omega_-^2)(\omega^2 - \omega_+^2)$$

$$\omega_{1,2}'^2 = \frac{\omega_{1,2}^2}{(1 - \frac{MS_{2,1}}{L_{2,1}S_{1,2}})} \qquad D = \frac{\mu_0^2}{L_1 L_2 - M^2}$$

$$\kappa = \frac{\omega^2 D k^3 [B_1(\omega^2 - \omega_1'^2) + B_2(\omega^2 - \omega_2'^2)]}{6\pi\mu_0} \tag{2.19}$$

Hence, the magnetic polarizability function is obtained for a SRR element as imposing (2.19) in (2.18). As mentioned before, SRR particles possess magneto electric behavior. For this reason, both dielectric permittivity and the magnetic permeability vectors are expected to be dependent to the electric and the magnetic polarizability vectors. Relevantly, for the purpose of developing permittivity or permeability function both polarization cases should be considered. In the following section, the electrical polarizability vector is going to be derived.

The electrical polarizability occurs due to local electric field E^{loc} in the environment. In order to induce electrical polarization on a loop antenna (ring of a SRR), there are two possible sets of wave orientation. First, consider the case when the electric field is oriented horizontally with respect to the loop element, then, considering the axis orientations in Fig 2-7, the electrical field should be applied along *x*-direction. In this case, the induced charges will mainly be concentrated around the splits at the opposing points and the charged at the edges of each split will be the same. For this reason, the polarizability component does not depend on the presence or absence of the split [7]. In this situation, the electric polarizability component a_{ee}^{xx} is denoted as quasi-static and relevantly *xx*-component of the electric polarizability for a single loop of SRR under a vertical electrical field condition is given in (2.20) as derived in [11] for a circular loop.

$$a_{QS} = -\frac{4SJ_1^{'}(ka)}{\omega\eta A_1(ka)} \tag{2.20}$$

Here, the term $S = \pi a^2$ is the effective loop area where $a = (a_1 + a_2) / 2$, $\eta = \sqrt{\mu_0 / \varepsilon\varepsilon_0}$ is the wave impedance of the host medium, $k = \omega\sqrt{\mu_0\varepsilon\varepsilon_0}$ is the wave number in that medium, $J_1^{'}(ka)$ is the derivative of the Bessel's function of the first kind and $A_1(ka)$ is the King's coefficient of the first mode. The King's coefficients are taken as denoted in [12] and [16] for a single loop antenna.

Equation (2.21) gives the approximate forms of King's coefficients for three modes. These three modes are all going to be used in further derivations.

$$A_0(ka) = \frac{ka}{\pi}(\log\frac{8a}{r_0} - 2) + \frac{0.667(ka)^3 - 0.267(ka)^5}{\pi} - j0.167(ka)^4 - j0.033(ka)^6$$

$$A_1(ka) = (\frac{ka - \frac{1}{ka}}{\pi})(\log\frac{8a}{r_0} - 2) - \frac{0.667(ka)^3 - 0.207(ka)^5}{\pi}$$
$$- j0.333(ka)^2 - j(0.133ka)^4 + j0.026(ka)^6$$

$$A_2(ka) = (\frac{ka - \frac{4}{ka}}{\pi})(\log\frac{8a}{r_0} - 0.667) + \frac{-0.4ka + 0.21(ka)^3 - 0.086(ka)^5}{\pi}$$
$$- j0.05(ka)^4 + j0.012(ka)^6 \qquad (2.21)$$

Above, the quasi-static electric polarizability is derived for a single loop however a SRR element is composed of two concentric loops. Therefore, the overall quasi-static electric polarizability term turns out to be the summation of polarizabilities of each loop given as in (2.22)

$$a_{ee}^{xx} = -\frac{4S_1 J_1^{'}(ka_1)}{\omega\eta A_1(ka_1)} - \frac{4S_2 J_1^{'}(ka_2)}{\omega\eta A_1(ka_2)} \qquad (2.22)$$

Now, let's consider another set of electric field orientation where it is applied in the vertical, i.e. in the *y*-direction as in Fig 2-7. In this case, the effects of the presence of the splits are taken into account and the *yy*-component of the electric polarizability is derived as (2.23). The detailed calculations could be found in [11].

$$a_{ee}^{yy} = \frac{4\pi a^2 J_1^{'}(ka)}{\omega\eta A_1(ka)}(1 + \frac{2j}{\pi\eta A_1(ka)}\frac{1}{Y_L + Y_{split}}) \qquad (2.23)$$

Here, Y_{split} is the admittance of the loop splits, $Y_{split} = j\omega C_{1,2}$ and $C_{1,2}$ is the total loop capacitance including as well the mutual interaction as mentioned previously. Y_L is the loop admittance, $Y_L = 1/ Z_L$. In order to build a more complete polarization function, the mutual interactions between the loops also contribute to the loop admittance term. The admittance of each loop is inversely proportional to the King's coefficient of three modes and the total loop admittances should be calculated by considering the mutual interaction term as well. The formula for the complete loop admittances of each loop is given in (2.24) considering the mutual interaction term.

$$\frac{1}{Y_1} = Z_1 = Z_{L1} + Z_{12}\frac{I_2}{I_1}$$

$$\frac{1}{Y_2} = Z_2 = Z_{L2} + Z_{12}\frac{I_1}{I_2}$$

$$Y_L = \frac{1}{j\pi\eta}\left(\frac{1}{A_0(ka)} + \frac{2}{A_1(ka)} + \frac{2}{A_2(ka)}\right) \tag{2.24}$$

where, $a=a_1$ and $a=a_2$ for outer and inner loops respectively, and $Z_{12} = j\omega M$ is the mutual inductance term. Following these notations the yy-component of the electric polarizability function turns out to be as in (2.25)

$$a_{e1}^{yy} = \frac{4S_1 J_1^{'}(ka_1)}{\omega\eta A_1(ka_1)}\left(1 + \frac{2j}{\pi\eta A_1(ka_1)}\frac{1}{Y_1 + j\omega C_1}\right)$$

$$a_{e1}^{yy} = \frac{4S_2 J_1^{'}(ka_2)}{\omega\eta A_1(ka_2)}\left(1 + \frac{2j}{\pi\eta A_1(ka_2)}\frac{1}{Y_2 + j\omega C_2}\right) \tag{2.25}$$

At this point, the only parameter left to be calculated is the current ratio term in the loop admittance function. Let's denote the current ratio term as $\xi = I_1 / I_2$. This term could be calculated by comparing the two sets of the electromotive force equations in (2-12). Hence, the current term is obtained as in (2.26)

$$\xi = \frac{\varepsilon_{E1}(Z_{L2} + Z_{C2}) - \varepsilon_{E2} Z_{12}}{\varepsilon_{E2}(Z_{L1} + Z_{C1}) - \varepsilon_{E1} Z_{12}} \tag{2.26}$$

From [11], when a single loop of impedance Z_L, loaded with the split impedance Z_{split}, is exposed to an external electric field in the yy-direction, the induced electromotive force on that loop could be calculated from (2.27)

$$\varepsilon_E = \frac{4aJ_1^{'}(ka)\left(\frac{1}{Y_L + Y_{split}}\right)}{j\eta A_1(ka)}\left(1 + \frac{j}{\pi\eta}\frac{1}{Y_1 + Y_{split}}\right)E_y^{loc} \tag{2.27}$$

The electromotive forces should be calculated for inner and outer loops separately since the radius of each loop differs. Thus the radius term in (2.27) should be the radius of each loops as $a = a_1$ and $a = a_2$. Consequently, by obtaining the yy-oriented electric polarizabilities of each loop, the total term could be obtained as the sum of these two polarizabilities as in (2.28)

$$a_{ee}^{yy} = a_{e1}^{yy} + a_{e2}^{yy} \tag{2.28}$$

Up to now, the magnetic and electric polarizabilities are derived for an individual SRR element under certain orientations of electric and magnetic fields. The effective (averaged) polarizability functions of a SRR are to be derived as well since the fields are chosen to be applied in certain directions. For this purpose, a SRR element is considered as a planar bianisotropic particle in an isotropic mixture. Then, the effective polarizabilities is obtained for a SRR by (2.29) since an isotropic mixture with a random orientation of particles can be considered as a mixture realized with isotropic particles which have averaged scalar polarizabilities [13]. The effective electric and magnetic polarizabilities can be calculated as in (2.29)

$$a_{ee}^{av} = \sum_{\alpha=1}^{3} \frac{a_{ee}^{\alpha\alpha}}{3}, \qquad a_{mm}^{av} = \sum_{\alpha=1}^{3} \frac{a_{mm}^{\alpha\alpha}}{3}, \qquad a_{em}^{av} = a_{me}^{av} = 0 \tag{2.29}$$

Here, the Cartesian designators are denoted as $\alpha = x, y, z$. As can be seen from the effective polarizability functions, SRR element does not have cross polarizability component because of the chosen orientation of the fields [7]. The effective (averaged) polarizabilities of a SRR element given in (2.29) are simulated by a Matlab code and the results are plotted in Fig. 2-8 and Fig. 2-9 for the magnetic and the electric polarizabilities, respectively. Comparing the real parts of the magnetic and the electric polarizabilities in Fig. 2-8 and Fig. 2-9, it is seen that the resonance band of the magnetic polarizability is around 4.4 GHz and the resonance of electric polarizability is around 3.8 GHz. This result is quite significant since the two resonances are observed not to overlap. Moreover, in Fig 2-8, the magnetic polarizability function indicates a single resonance band around 4.4 GHz, which is expected since the two eigenmodes are to be overlapped, i.e. $\omega_{+} \approx \omega_{-}$. However, in Fig 2-9, the electric polarizability results give an additional resonance band around 4 GHz which is in fact not expected. In [7], this defect is said to be risen because of some lack of approximating the parameters in the mutual capacitance term C_{mut}. The developed analytical model is validated via experimental results in [7] and the analytical model results are observed to give perfect agreement with the experimental data. Moreover in [7], it is seen that this additional resonance band does not possess any significant effect in simulating the electrical polarizability response.

Up to now, the analytical functions of the electric and the magnetic polarization vectors of a SRR element are derived. Further, the electric permittivity and the magnetic permeability functions are going to be obtained by the help of already derived polarization vectors. As denoted previously, a SRR particle possesses magneto electric coupling i.e. external electric or magnetic fields alone induce both electric and magnetic dipoles in the SRR particle. In [13], the relationship between the averaged polarizabilities and the effective medium parameters for an isotropic mixture is given by the Maxwell Garnett formulas as presented in (2.30) for a loop antenna.

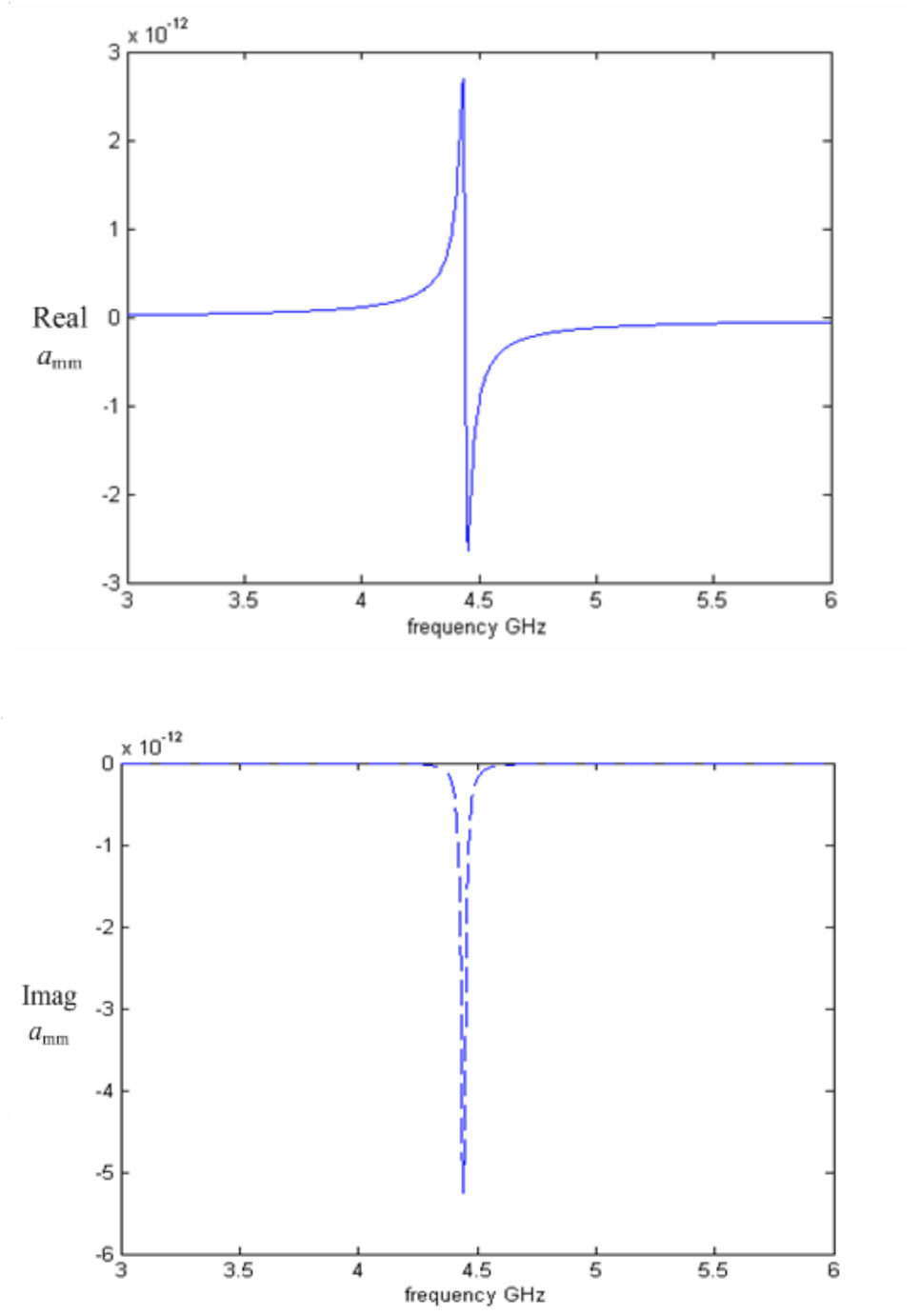

Figure 2-8: The simulation results for real (solid) and the imaginary (dashed) parts of the averaged magnetic polarizability of a random SRR.

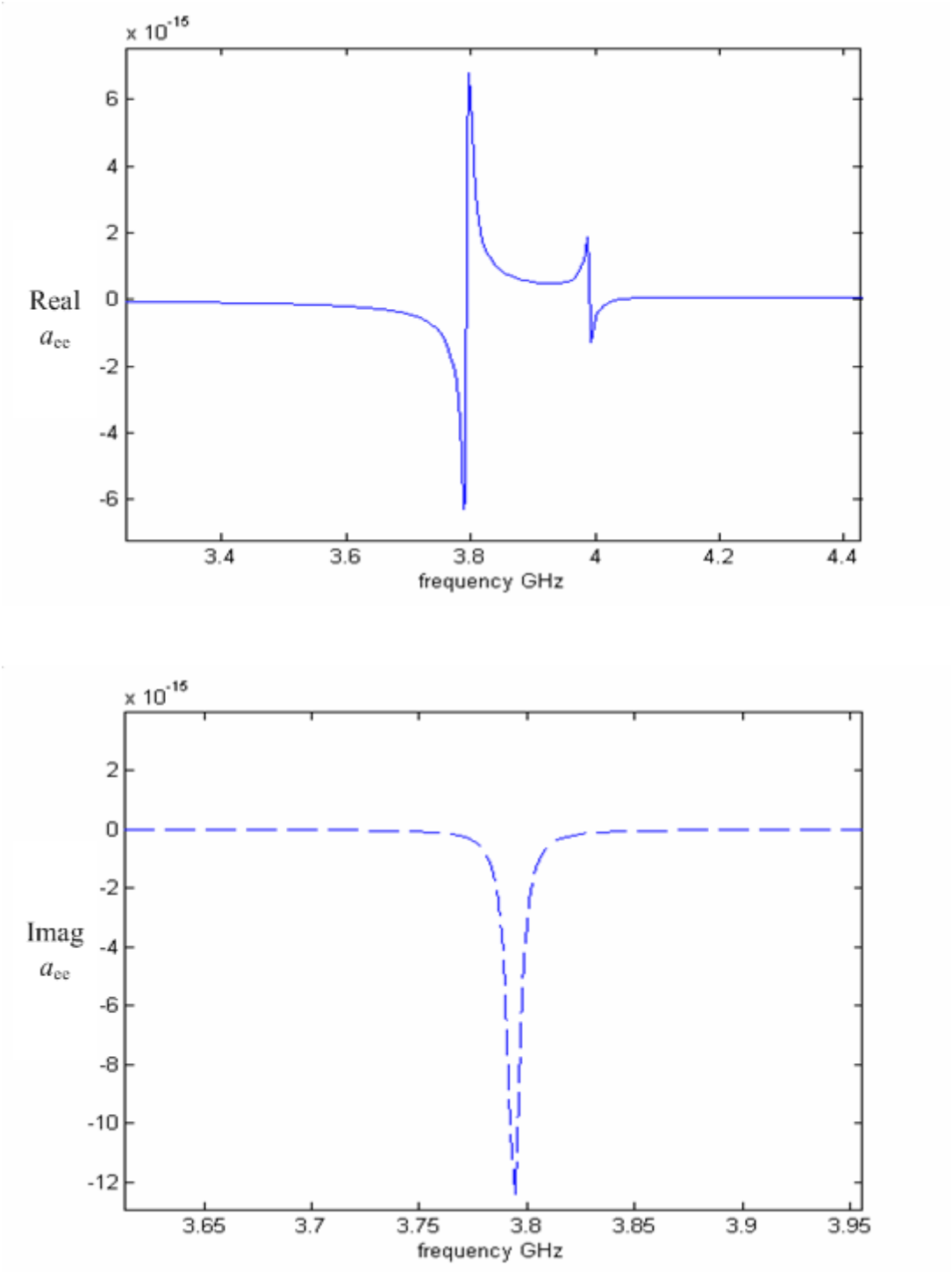

Figure 2-9: The simulation results for real (solid) and the imaginary (dashed) parts of the averaged electric polarizability of a random SRR.

Then, the permittivity and the permeability functions of a SRR are obtained to be dependent on both the electric and the magnetic polarizabilities as in (2.30) by using the Maxwell Garnett formulas.

$$\varepsilon_{eff} = \varepsilon + F\left(\frac{Na_{ee}^{'}}{\varepsilon_0} - \frac{N^2 a_{ee}^{'} a_{mm}^{'}}{3\varepsilon_0 \mu_0}\right)$$

$$\mu_{eff} = 1 + F\left(\frac{Na_{mm}^{'}}{\mu_0} - \frac{N^2 a_{ee}^{'} a_{mm}^{'}}{3\varepsilon_0 \mu_0 \varepsilon}\right)$$

and

$$F^{-1} = 1 - \frac{Na_{ee}^{'}}{3\varepsilon_0 \varepsilon} - \frac{Na_{mm}^{'}}{3\mu_0} + \frac{N^2 a_{ee}^{'} a_{mm}^{'}}{9\varepsilon_0 \mu_0 \varepsilon} \qquad (2.30)$$

where the term N presents the concentration of particles. For a single SRR element, the permittivity and the permeability functions are obtained via comparing (2.29) and (2.30). Then, they are simulated by a Matlab code. The simulation results for the effective permittivity and the permeability of a SRR are given in Fig 2-10 and Fig 2-11, respectively. Throughout the computations, concentration of the particles are taken to be N=1 particle/cm^3. In Fig. 2-10, there is an additional resonance similar to the electric polarizability function however, as denoted in [7], this resonance is due to lack approximation of the mutual interaction term. It is also worth to note that, similar to the polarizability case, the permittivity and the permeability functions have the resonances around different frequencies.

For further investigation of the electric and magnetic responses, the SRR particles are assumed to be in a periodic geometry. The periodicity is obtained in a three dimensional cubic geometry as illustrated in Fig 2-12. In the model derivation, the SRRs are assumed to form a distribution of infinite extent through each axis.

In this case, an electric field directed along an arbitrary edge of a cubic cell excites the electric dipoles in four SRR particles. For two particles E_{loc} is parallel to the line connecting the rings splits and corresponds to the polarizability a_{ee}^{xx}. For the other

two particles E_{loc} is perpendicular to this line and corresponds to a_{ee}^{yy}. Similarly, a magnetic field directed along an arbitrary edge of a cell induces two equivalent magnetic moments in two opposite particles. So, the magnetic polarizability of a unit cell turns out to be the double of a_{mm}^{zz} [7]. Thus the cubic cell of interest could be considered as an isotropic particle with electric and magnetic polarizabilities as in the form (2-31). Then, Maxwell Garnett formulas (2.30) are used to derive the effective medium parameters for the periodic SRR structure and obtained model is simulated by a Matlab code.

$$a_{ee}' = 2a_{ee}^{xx} + 2a_{ee}^{yy} \qquad a_{mm}' = 2a_{mm}^{zz} \tag{2.31}$$

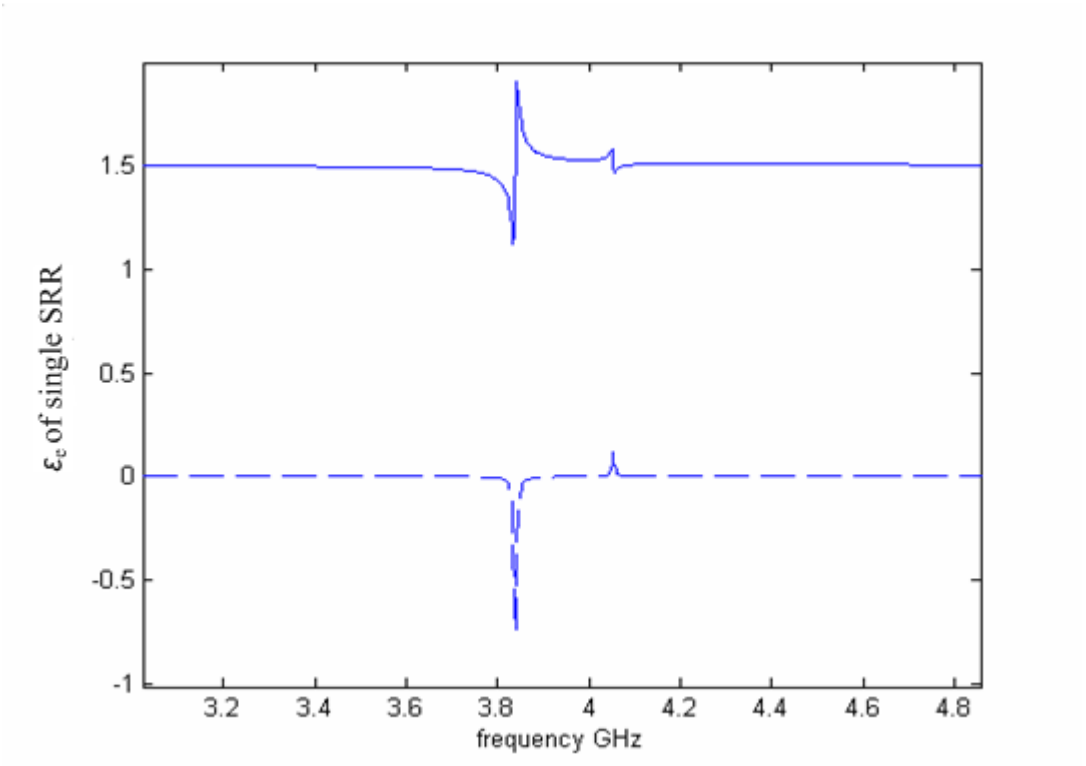

Figure 2-10: Effective permittivity simulation results for a random SRR. Real (solid) and the imaginary (dashed) parts are presented

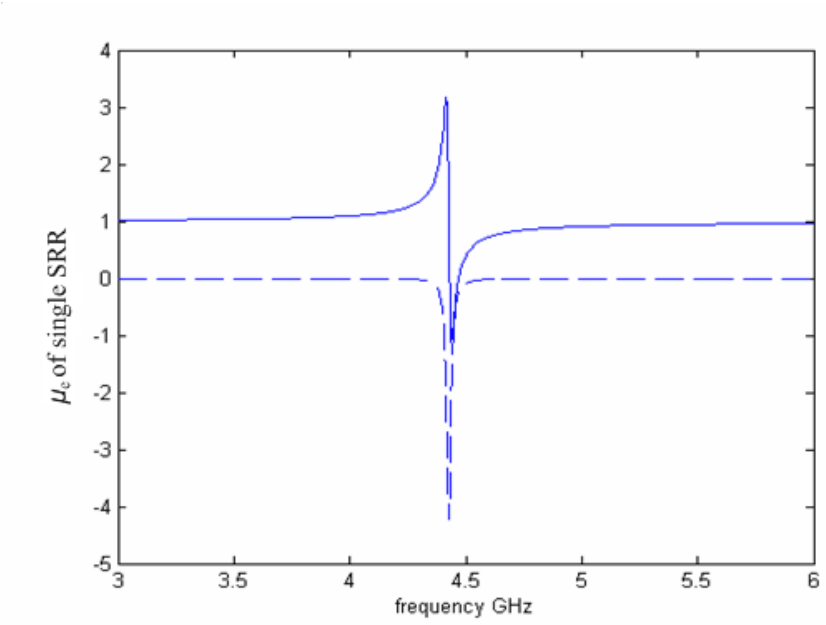

Figure 2-11: Effective permeability simulation results for a random SRR. Real (solid) and the imaginary (dashed) parts are presented

Figure 2-12: The cubic cell presentation suggested for the derivation of effective medium parameters [7]

In Fig. 2-13, the effective permittivity results are presented for the periodic SRR structure and it is observed to possess a resonance band around 3.8 GHz. The permittivity function is observed to have an additional resonance behavior similar to the previous observations. This defect also raises from insufficient approximation of the mutual interaction terms and as discussed previously it indicates no significant

effect on the model. Then, in Fig. 2-14, the simulation results for the effective permeability is presented which show a resonance behavior around 4.4 GHz. Although the SRR particles are said to have magneto electric coupling, the electric polarizability and the permittivity functions indicate the resonance behavior around the same frequency, 3,8 GHz for our model. This observation is also valid for the magnetic case since the magnetic polarizability and the permeability functions possess the resonance behavior around the same frequency, 4.4 GHz in our model. It is evident from Fig 2-13 and Fig 2-14 that for the cubic model of concern, the electric permittivity and the magnetic permeability resonance bands do not overlap. Moreover, the permittivity and permeability functions cannot be altered individually since they are highly dependent on the same parameters of the SRR itself or of the host medium. Considering this fact, another artificial structure, the thin wire array, is used in order to obtain the desired metamaterial parameters. In the following section the thin wire arrays will be studied for the purpose of obtaining the desired permittivity behavior.

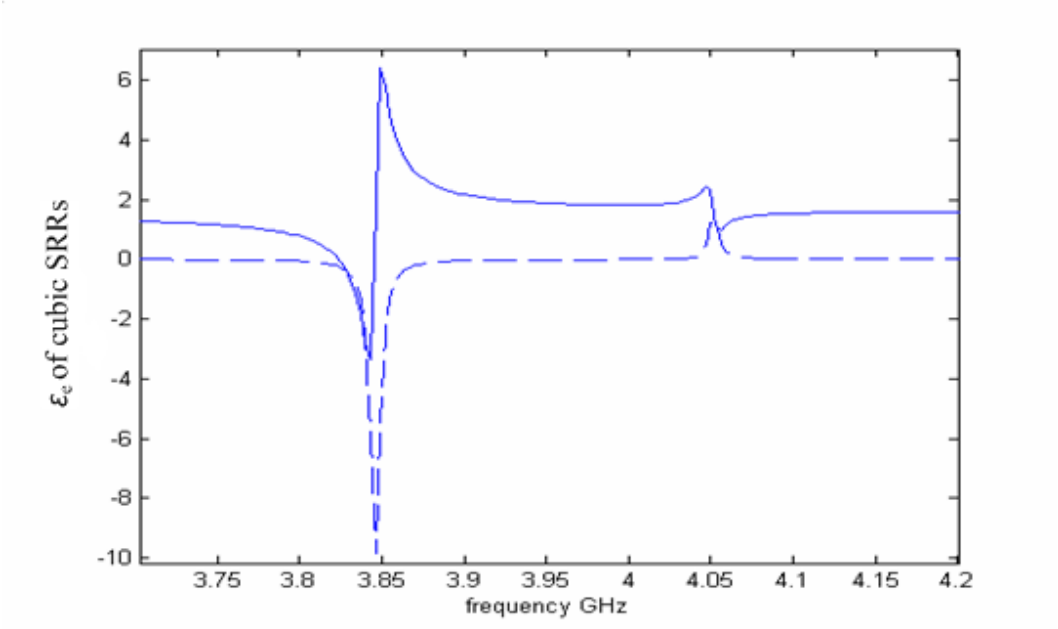

Figure 2-13: Effective permittivity simulation results for the proposed cubic cell. The real (solid) and the imaginary (dashed) parts are presented

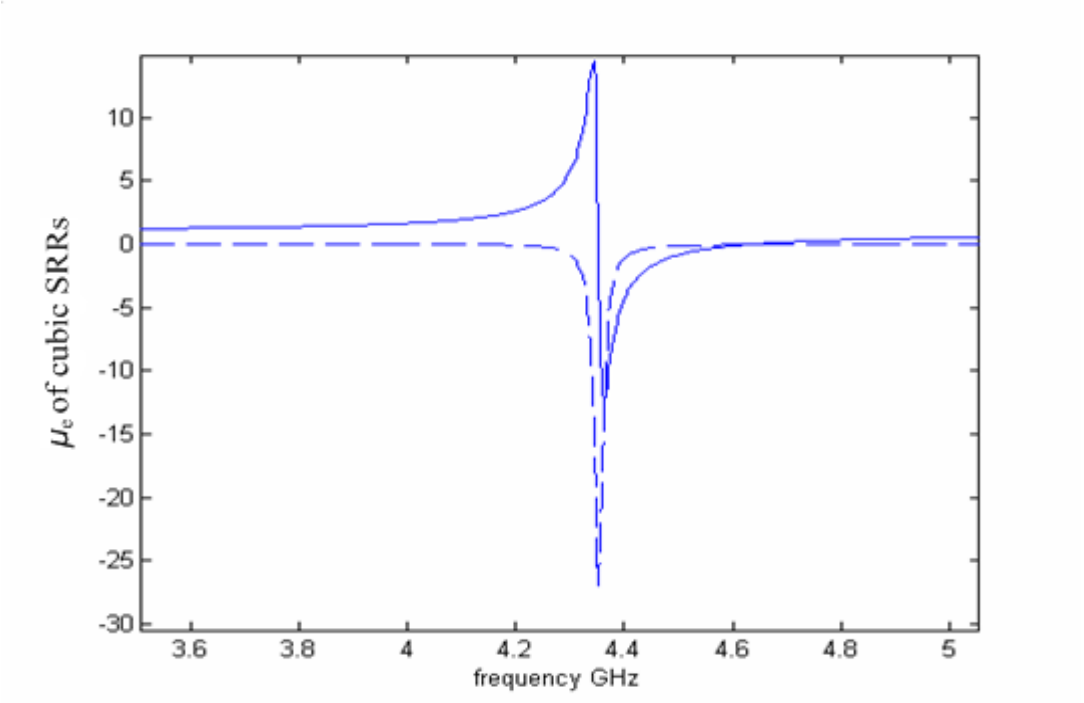

Figure 2-14: Effective permeability simulation results for the proposed cubic cell. The real(solid) and the imaginary(dashed) parts are presented

CHAPTER 3

OBTAINING NEGATIVE PERMITTIVITY

In the previous chapter the negative permeability phenomenon is studied through a recently introduced metamaterial structure namely Split Ring Resonator. For this structure, the models of permittivity and permeability functions are studied. It is seen from the simulation results that the derived electric and magnetic characteristics of SRR (i.e., the negative permittivity and permeability parameters) cannot be obtained over a common frequency band. For this reason another metamaterial structure is needed to be used in combination with the SRRs

The plasma medium is known to possess negative permittivity behavior under a certain frequency called the plasma frequency [6]. For natural plasma, the plasma frequency is seen in near UV or visible region. In this chapter, the negative permittivity characteristic of the plasma medium, simulated by an artificial metallic wire array, will be studied.

Plasma is basically described as an ionized medium with an equal concentration of mobile negative and positive charges. Relevantly, the charges in plasma are expected to be polarized by applying an external field. Suppose that in plasma there are N molecules per unit volume. Each electron in the plasma will contribute to the overall dielectric function with a binding frequency of ω_j and damping constant γ_j as in (3.1). Here, m is the molecular weight and f_j is the number of electrons per molecule [17].

$$\frac{\varepsilon(\omega)}{\varepsilon_0} = 1 + \frac{\mathrm{Ne}^2}{\varepsilon_0 m} \sum_j f_j (\omega_j{}^2 - \omega^2 - i\omega\gamma_j)^{-1} \tag{3.1}$$

Then, above the plasma resonance frequency, the dielectric function of the plasma turns out to have the compact form given in (3.2)

$$\varepsilon(\omega) = 1 - \frac{\omega_p^2}{\omega(\omega + j\gamma)} \tag{3.2}$$

where ω_p is the plasma frequency and γ is a damping term presenting the dissipation of the plasmon's energy in the system [17]. It could be seen that the real part of $\varepsilon(\omega)$ is negative below the plasma frequency ω_p.

In equilibrium, the charge on the electron gas of plasma is compensated by the background nuclear charge. If an external field $E(x,t)$ is applied to the plasma, this field bounds the charges with a restoring force as in (3.3)

$$\mathbf{F} = - m\omega_o x \tag{3.3}$$

where m is the mass of the charge, ω_o is the frequency of oscillation and x is the position vector [17]. Removing the plasma from the system, a surplus of uncompensated charge is generated at the ends of the medium, with opposite signs at opposite ends supplying a restoring force resulting in simple harmonic motion with the frequency, ω_p. This frequency is then called the plasma frequency [2].

$$\omega_p{}^2 = \frac{n_{eff} e^2}{\varepsilon_0 m_{eff}} \tag{3.4}$$

where n_{eff} is the effective density of the charge and m_{eff} is effective mass of the charged specimen.

As denoted previously, for natural plasma, the plasma frequency is seen in near UV or visible region. Considering (3.4), it looks possible to lower the plasma frequency. However, there exists a restriction that the plasmon behavior would not be violated for plasma applications. The plasmon is basically the quasiparticle resulting from the quantization of plasma oscillations, typically observed in the visible and near UV region [2]. However, at much lower frequencies dissipation violates the well established collective excitation behavior of plasmons. In 1996, J. B. Pendry suggested a model in order to lower the plasma frequency into the far infrared or even GHz band by keeping the plasmon behavior. His method was increasing the effective mass of the electrons in plasma and relevantly reducing the plasma frequency. In doing so, he studied the thin wire array which was already known to be able to simulate the plasma medium [7]. In Fig. 3-1 the wire array structure studied by Pendy in [2] is shown where ***r*** is the element radius and ***a*** is the lattice constant.

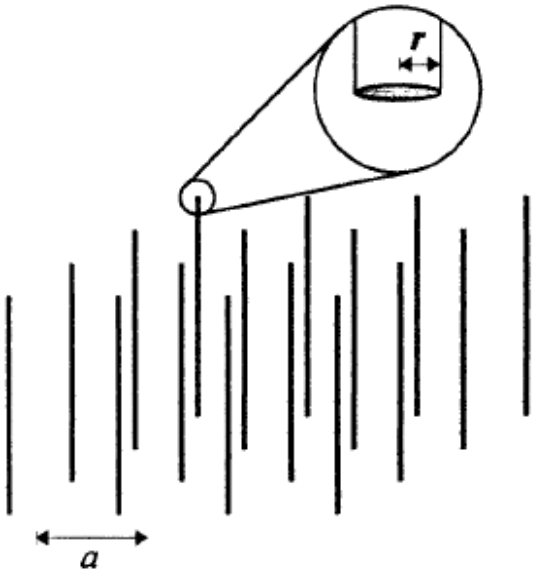

Figure 3-1: An array of wires aligned as a square lattice [2]

Consider now the wire array presented in Fig. 3-1. If the density of electrons in a single wire is *n*, the density of these electrons in the structure as a whole is given by the fraction of space occupied by wire.

$$n_{eff} = n\frac{\pi r^2}{a^2} \tag{3.5}$$

Additionally, the effect of interactions among the electrons in the wire structure on a single electron will contribute to the mass of that electron, hence the effective electron mass will increase [2]. Suppose now a current $I = nve$ is flowing in a wire, creating a magnetic field circling the wire,

$$H(R) = \frac{1}{2\pi R} = \frac{\pi r^2 nve}{2\pi R} \tag{3.6}$$

where R is the distance from the wire center, v is the electron velocity, and ne is the charge density. In term of vector potential, the magnetic field expression can also be rewritten as

$$H(R) = \mu_0^{-1}\nabla \times A(R) \tag{3.7}$$

where

$$A(R) = \frac{\mu_0 \pi r^2 nve}{2\pi}\ln(a/R) \tag{3.8}$$

Under an external magnetic field, each electron would have an additional contribution on its own momentum of $e\boldsymbol{A}$ [2], and therefore the momentum per unit length of the wire could be written as in (3.9).

$$e\pi r^2 nA(r) = \frac{\mu_0 e^2 (\pi r^2 n)^2 v}{2\pi}\ln(a/r) = m_{eff}\pi r^2 nv \tag{3.9}$$

where m_{eff} is the effective mass of the electrons and note that the interactions among the electrons are as well considered. Comparing both sides of (3.9), the effective mass formula could be obtained as in (3.10)

$$m_{eff} = \frac{\mu_0 e^2 \pi r^2 n}{2\pi} \ln(a/r) \tag{3.10}$$

Finally, the effective mass formula in (3.10) would be substituted into (3.4) for the purpose of obtaining the effective plasma frequency as in (3.11)

$$\omega_p{}^2 = \frac{n_{eff} e^2}{\varepsilon_0 m_{eff}} = \frac{2\pi c_0{}^2}{a^2 \ln(a/r)} \tag{3.11}$$

It is worth to note that although the reduced plasma frequency can be expressed in terms of electron effective mass and charge, these microscopic quantities cancel out and leave a formula containing only macroscopic parameters of the structure which are the wire radius r and the lattice spacing a. The plasma frequency can now be tuned to GHz frequency band. However, one should consider the restriction that the wire radius r and the lattice spacing a must be much smaller than the wavelength of the radiation in order to preserve the plasmon condition of the plasma.

Hence, substituting the damping term γ to (3.2) as given in [2], the effective dielectric function can be written as in (3.12) where σ is the conductivity of the wire material.

$$\varepsilon_{eff} = 1 - \frac{\omega_p{}^2}{\omega(\omega + j\varepsilon_0 a^2 \omega_p{}^2 / \pi r^2 \sigma)} \tag{3.12}$$

The derived effective permittivity and the plasma frequency formulas are simulated by a Matlab code written. In the computations, the wires are chosen to be aluminum where the element radius r = 1.0 x 10^{-6} m and the lattice constant a = 5.0 x 10^{-3} m.

The density of electrons in a single aluminum wire is taken as n = 1.806 x 10^{29} m^{-1}, then the corresponding effective mass of electrons becomes

$$m_{eff} = 2.4808 \text{ x } 10^{-26} \text{ kg} = 2.7233 \text{ x } 10^{4}\, m_e \tag{3.13}$$

In (3.13), m_e is the mass of an electron where m_e=9.1094 x 10^{-31} kg. Equation (3.13) shows that the effective electron mass is enhanced by 4 orders of magnitude by increasing the electron density through the wires. The relevant plasma frequency then turns out to be ω_p = 5.1534 x 10^{10} t^{-1} or $f_p \approx 8.2$ GHz. For our example, the wires are chosen to be made of aluminum then the conductivity term is σ = 3.65 x 10^{7} Ω^{-1} m^{-1}. Consequently, substituting these parameters into (3.12), the resulting effective permittivity could be obtained in the compact form given in (3.14).

$$\varepsilon_{eff} \approx 1 - \frac{\omega_p^{\,2}}{\omega(\omega + j0.1\omega_p)} \tag{3.14}$$

The effective permittivity function derived in (3.14) is simulated by a Matlab code and the resulting function is presented in Fig. 3-2. It is seen from the figure that the real part of effective permittivity becomes negative below the plasma frequency which is previously calculated as 8.2 GHz for our example. The real part of permittivity tends to converge to unity above the plasma frequency while the imaginary part vanishes as frequency increases.

In Fig. 3-3, the dispersion graph for the array of aluminum wires is presented considering the dielectric function in (3.2). As seen from the figure, the real bands are obtained only above and imaginary bands below the plasma frequency, which is 8.2 GHz in our case. The results also predict a plasmon behavior with a wave vector expression satisfying the equation (3.15)

$$\kappa = \omega \frac{\sqrt{\varepsilon_{eff}}}{c_0} \tag{3.15}$$

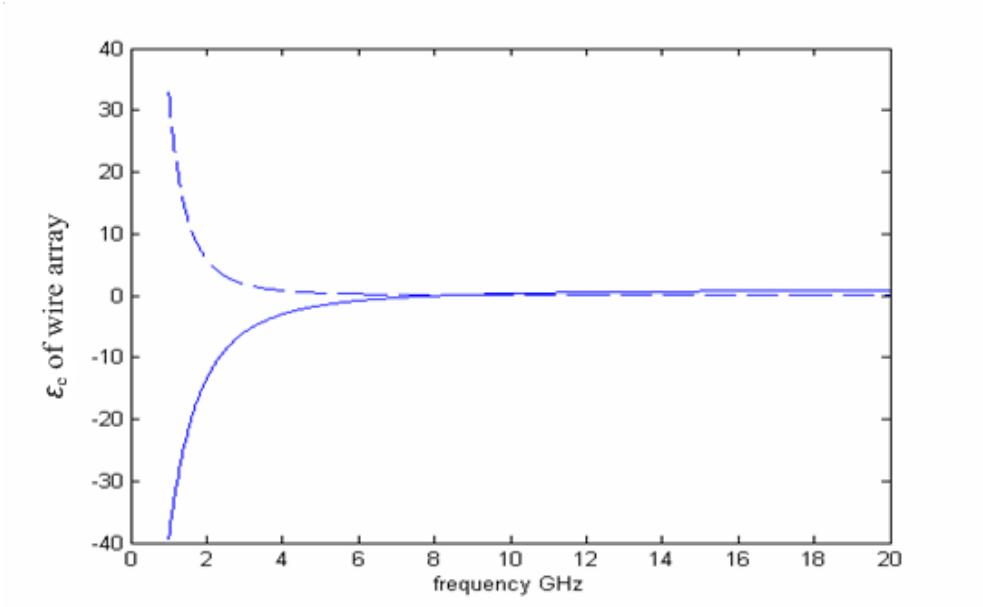

Figure 3-2: Simulation of the permittivity for an aluminum wire array; real (solid) and imaginary (dashed) parts are presented

Computed wave vector agrees very well at $\kappa = 0$, but shows a small degree of dispersion towards the Brillouin zone boundary. In Fig. 3-3, the dispersion around the boundary could also be seen accurately [2].

As far as external electromagnetic radiation is concerned, the thin wire structure would be modeled as an effectively homogenous dielectric medium. For this respect it is quite important that the structure is made of thin wires. Moreover, considering the derived plasma frequency formula in (3.11), small radius is needed also to reduce the plasma frequency.

On the contrary, in the case of an array of thick wires, $ln(a/r) \approx 1$ thus the plasma frequency corresponds to a free space wavelength of nearly twice the lattice parameter *a*. Therefore Bragg diffraction effects would violate the desired plasmon picture. Small radius ensures that Bragg diffraction occurs only at much higher frequencies.

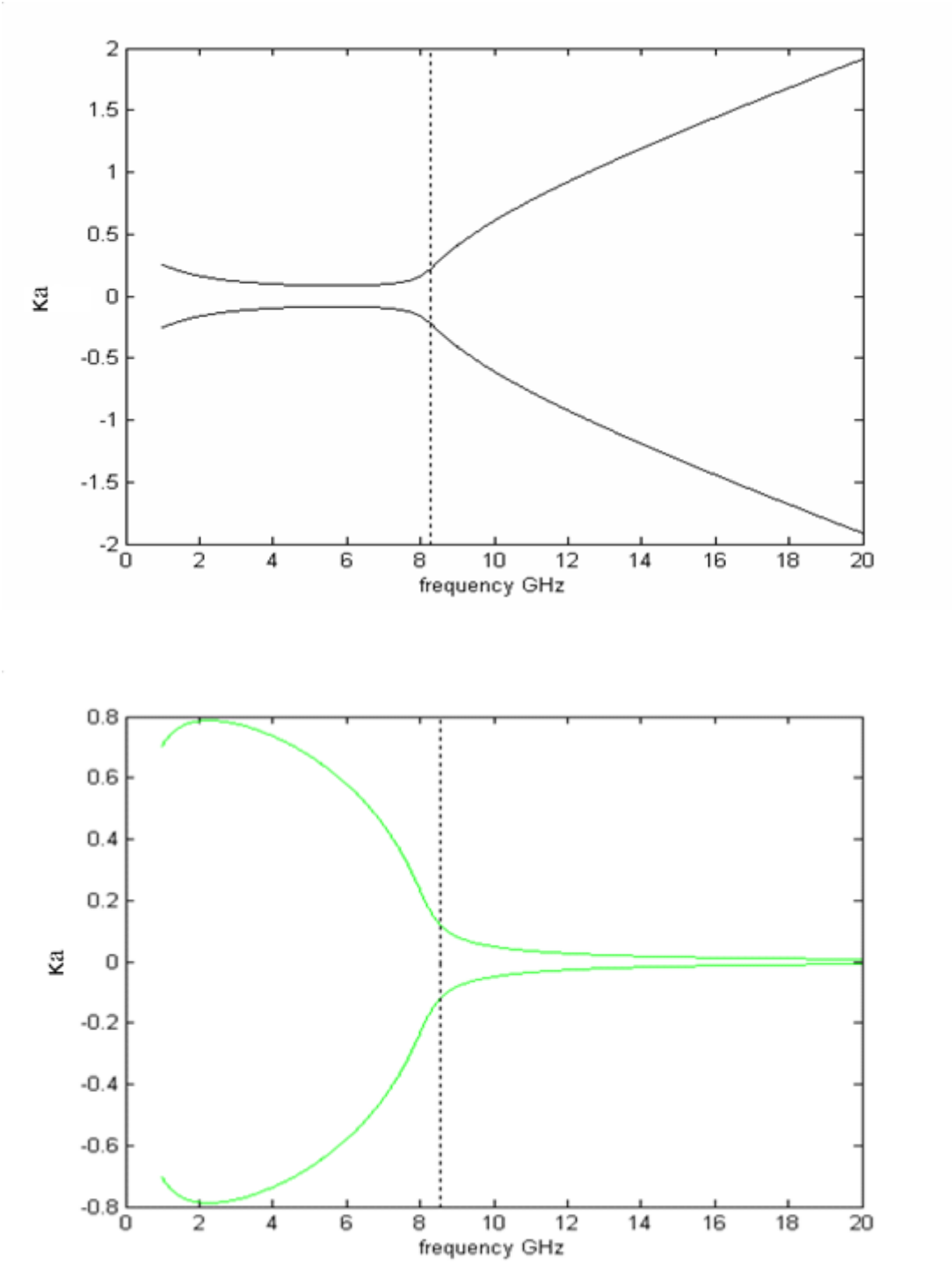

Figure 3-3: Numerical simulations of the band structure for aluminum wire array where real (top) and imaginary (bottom) parts of κa are shown

J. B. Pendry's innovative inferences, discussed so far, attracted plenty of academic interest and influenced many studies especially in late 1990s. One of the most significant of those came from Harbin Institute of Technology in China [8]. The Chinese group indented to improve the studies of Pendry in a way that the metallic wire array is no longer need to be in square symmetry. In doing so, they first derived the transmission line equivalent model for the periodic wires and solved for the desired permittivity function by the help of transmission line theory. Thin wires are modeled as inductive elements where different lattice spacings can be chosen at different axes. The inductor array equivalent of metallic wires is presented in Fig. 3-4. In this inductor model, the wire spacing through the *x*-axis may differ from the one in the *y*-axis which is the basic improvement compared to Pendry's model. In the rest of this chapter, the studies of Harbin Institute of Technology are going to be summarized and the permittivity function of their model will be simulated using a Matlab code.

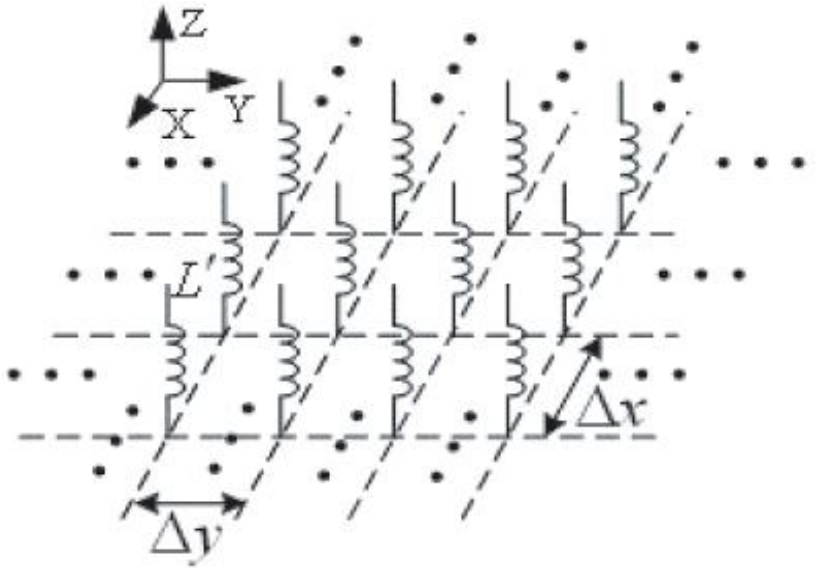

Figure3-4: Inductor Array equivalent of the thin wire array [8]

Considering the notations in Fig. 3-4; L' is the wire self-inductance per unit length in z direction, and Δx and Δy are the wire spacing in x and y directions as given in [8]. It is worth to note that in the case of equivalent wire spacing $\Delta x = \Delta y = a$, the new model becomes the same as the one in Pendry's study. Therefore, the new model might also be verified via comparing its square symmetric case with the Pendry's model.

In this model, the average inductance of the array in the x-y plane is described by the inductance per unit area type density relating the macro effects of thin wire array to the size parameters [8] as in (3.16)

$$L_s = L'\Delta x\Delta y = \mu_0 \frac{\ln(\Delta x / r)\ln(\Delta y / r)}{\pi\left[\ln(\Delta x / r) + \ln(\Delta y / r)\right]}\Delta x\Delta y \tag{3.16}$$

Suppose that free space plane electromagnetic waves in (3.17) are present in the medium of interest.

$$\vec{\mathrm{E}} = \vec{\alpha}_z \mathrm{E}_0 e^{-j\beta y}$$

$$\vec{H} = \vec{\alpha}_x H_0 e^{-j\beta y} \tag{3.17}$$

Here, $\vec{\alpha}_z$ and $\vec{\alpha}_x$ are the unit vectors, β is the propagation constant in free space, E_0 and H_0 are the amplitude of the electric and the magnetic fields, respectively. Consider now if a parallel-plate waveguide infinite in the x-y plane is placed perpendicularly to the electric field direction as indicated in Fig. 3-5, the internal field distribution of overall wire array does not change and this internal field can be described by the voltage between the two plates, and the surface current on the inner sides of the plates [8].

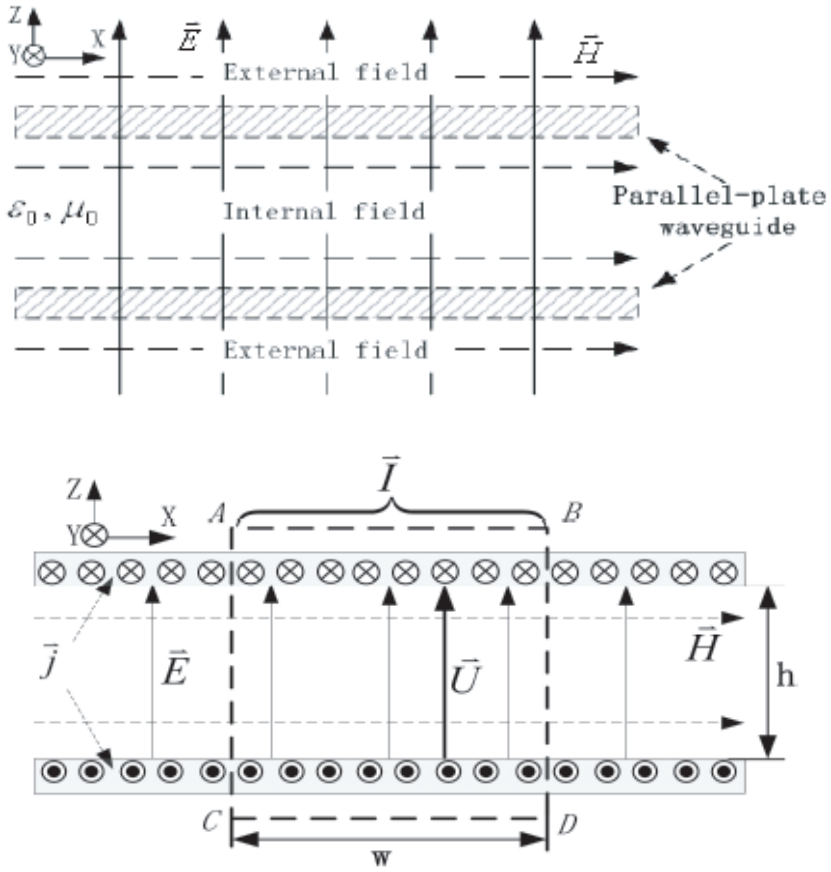

Figure 3-5: Wire array vertically standing between opposing metal plates (top) and relevant parameter presentations (bottom) [8]

The ABCD region in Fig. 3-5 is considered as a unit element since the array is supposed to be uniform in *x* and *y* directions. Then using the transmission line theory the current $\vec{I}$ and the voltage $\vec{U}$ in the region ABCD may be obtained as in (3.18) and (3.19), respectively.

$$\vec{I} = \omega\vec{j} = \omega\vec{\alpha}_z \times \vec{H} = \vec{\alpha}_y \omega H_0 e^{-j\beta y} \tag{3.18}$$

and

$$\vec{U} = h\vec{E} = \vec{\alpha}_z h E_0 e^{-j\beta y} \tag{3.19}$$

where *w* is the length of the line segment CD, *h* is the distance between the two plates and $\vec{j}$ is the surface current on the internal faces of the parallel plate waveguide . Note that the propagation constant for free space is (3.20).

$$\beta = \omega\sqrt{\varepsilon_0\mu_0} = \omega\sqrt{L_0C_0}\,. \tag{3.20}$$

The characteristic impedance between the two bounding plates may be obtained by dividing the voltage term in (3.19) to the current term in (3.18).

$$Z = \frac{\vec{U}}{\vec{I}} = \frac{h}{\omega}\frac{\mathrm{E}_0}{H_0} = \frac{h}{\omega}\sqrt{\frac{\mu_0}{\varepsilon_0}} = \sqrt{\frac{L_0}{C_0}} \tag{3.21}$$

Here, C_0 and L_0 are the distributed capacitance and inductance per unit length of the transmission line equivalence of the ABCD region. Therefore the capacitance and the inductance terms may be obtained by considering (3.20) and (3.21) as in (3.22)

$$L_0 = \frac{h\mu_0}{\omega} \qquad \text{and} \qquad C_0 = \frac{\omega\varepsilon_0}{h} \tag{3.22}$$

Calculating the capacitance and the inductance per unit length, the transmission line equivalence is obtained as in Fig. 3-6 for the unit cell, ABCD.

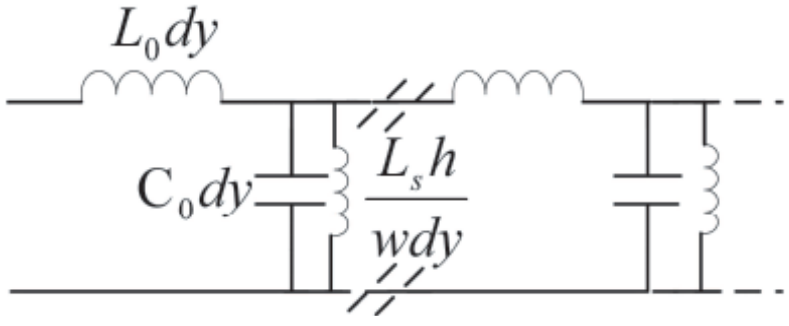

Figure 3-6: Equivalent unit circuit of the thin wire array [8]

Considering Fig. 3-6, the equivalent shunt admittance and the equivalent shunt inductance per unit length are calculated as in (3.23) and (3.24) respectively.

$$Z = \frac{1}{G} = \frac{1}{j\omega\frac{\omega\varepsilon_0}{h} + \frac{\omega}{j\omega h L_s}} = j\omega\frac{-1}{\omega^2\frac{\omega}{h}(\varepsilon_0 - \frac{1}{\omega^2 L_s})} \tag{3.23}$$

$$L_{eq} = \frac{-1}{\omega^2\frac{\omega}{h}(\varepsilon_0 - \frac{1}{\omega^2 L_s})} \tag{3.24}$$

Up to now, the equivalent circuit model for periodic metallic wires is obtained and the equivalent inductance and admittance parameters per unit length are derived from this circuit. Then, these circuit parameters are combined with the results of another significant study done by Caloz *et.* al in 2002 [14]. In his study, Caloz derived a compact formula for the effective permittivity of a wire array under the same set of external fields in (3.17)

$$\varepsilon_{eff} = -\frac{1}{\omega^2 L_{eq}\frac{\omega}{h}} \tag{3.25}$$

Hence, by substituting the derived equivalent inductance term (3.24) into Caloz's dielectric function (3.25), the effective permittivity may also be rewritten as (3.26)

$$\varepsilon_{eff} = -\frac{1}{\omega^2 L_{eq}\frac{\omega}{h}} = 1 - \frac{1}{\omega^2 L_s \varepsilon_0} = 1 - \frac{{\omega_p}^2}{\omega^2} \tag{3.26}$$

where ω_p is the resonant plasma frequency as mentioned previously. From (3.16), the inductance area density L_s is obtained as totally dependent to the lattice spacing and the wire radius. Thus it would be possible to obtain a compact permittivity function which is dependent only on the same size parameters as L_s does.

Relevantly, comparing the plasma dielectric function to the recently derived one in (3.26) yields a plasma frequency equation as in (3.27)

$$\omega_p{}^2 = \frac{1}{L_s \varepsilon_0} = \frac{1}{\Delta x \Delta y L' \varepsilon_0} \tag{3.27}$$

It is evident from (3.27) that in the case of square symmetry, $\Delta x = \Delta y = a$, the plasma frequency turns out to be as in (3.28):

$$\omega_p{}^2 = \frac{1}{a^2 L' \varepsilon_0} \tag{3.28}$$

Considering the reference square array of aluminum wires where the wire radius is r = 1 μm and the lattice spacing is a = 5 mm as chosen previously, the dispersion graph for such an array is simulated by a Maltab code and the simulation result is given in Fig 3-7. It is seen from the figure that the transmission line approach shows perfect agreement with the Pendry's plasmon approach. Therefore, the transmission line approach may be considered as an improved version of Pendry's approach in a way that the wire array is no longer in need of having square symmetry.

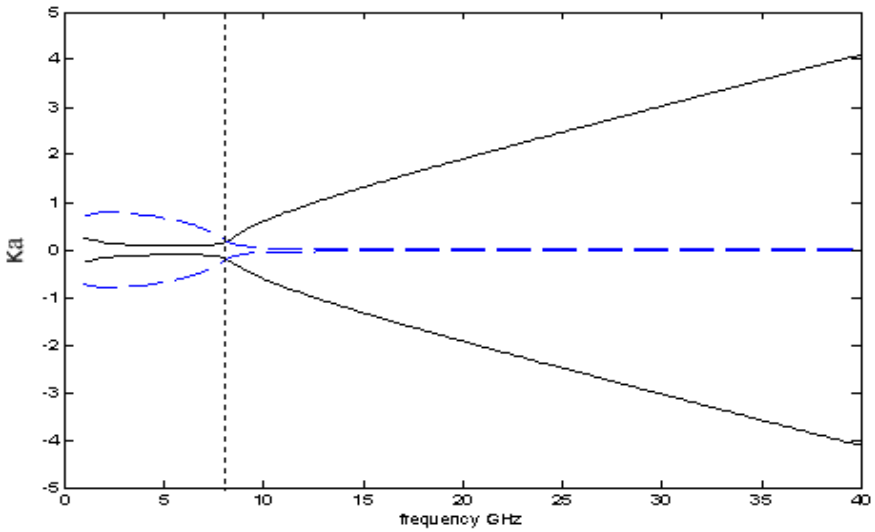

Figure 3-7: Numerical simulations of the band structure for aluminum wire array, real (solid) and imaginary (dashed) parts of the wave vector are presented.

CHAPTER 4

COMPOSITE METAMATERIAL HAVING NEGATIVE PERMITTIVITY AND NEGATIVE PERMEABILITY CONCURRENTLY

Up to this chapter, permeability and permittivity characteristics of the split ring resonators and the metallic wire arrays are examined individually. The observations indicated that the SRR structure is capable of yielding a frequency band with negative permeability but it can provide a much narrower frequency band with negative permittivity. The analytical simulation results are shown in Fig. 4-1 for the electric and the magnetic parameters of a SRR structure of cubic periodicity. As seen from Fig 4-2, the electric and magnetic resonances cannot be overlapped. Considering the analytical functions derived for SRR structures in Chapter-2, both the permittivity and permeability parameters are observed to be highly dependent to structure the parameters of the SRR. Thus attempts to overlap negative permittivity and negative permeability regions fail as the respective frequency bands shift in a similar way [7].

The metallic wire array on the other hand exhibits a wide range of negative electric permittivity region under the plasma frequency. In Fig 4-2, the permittivity function of an aluminum wire array is presented using the structure discussed in Chapter-3. For the sake of coherence, the array parameters are taken the same as in Chapter-3

where element radius $\boldsymbol{r}$ = 1.0 x 10^{-6} m and the lattice constant of $\boldsymbol{a}$ = 5.0 x 10^{-3} m. Since the wires are chosen to be aluminum, the density of electrons in one aluminum wire is calculated as n = 1.806 x 10^{29} m^{-1}, yielding an effective mass of $\boldsymbol{m_{eff}}$ = 2.4808 x 10^{-26} kg. Then using the effective permittivity formula (4.1), the permittivity function for the array of aluminum wires is obtained as in Fig. 4.2.

$$\varepsilon_{eff} = 1 - \frac{\omega_p{}^2}{\omega(\omega + i\varepsilon_0 a^2 \omega_p{}^2 / \pi r^2 \sigma)} \tag{4.1}$$

where σ is the conductivity of the wire material and ω_p is the plasma frequency as in the form (4.2). The permittivity function in Fig 4-2 is observed to take negative values below the plasma frequency where the resulting plasma frequency is calculated as ω_p = 5.1534 x 10^{10} t^{-1} or $f_p \approx 8.2$ GHz.

$$\omega_p{}^2 = \frac{n_{eff} e^2}{\varepsilon_0 m_{eff}} = \frac{2\pi c_0{}^2}{a^2 \ln(a/r)} \tag{4.2}$$

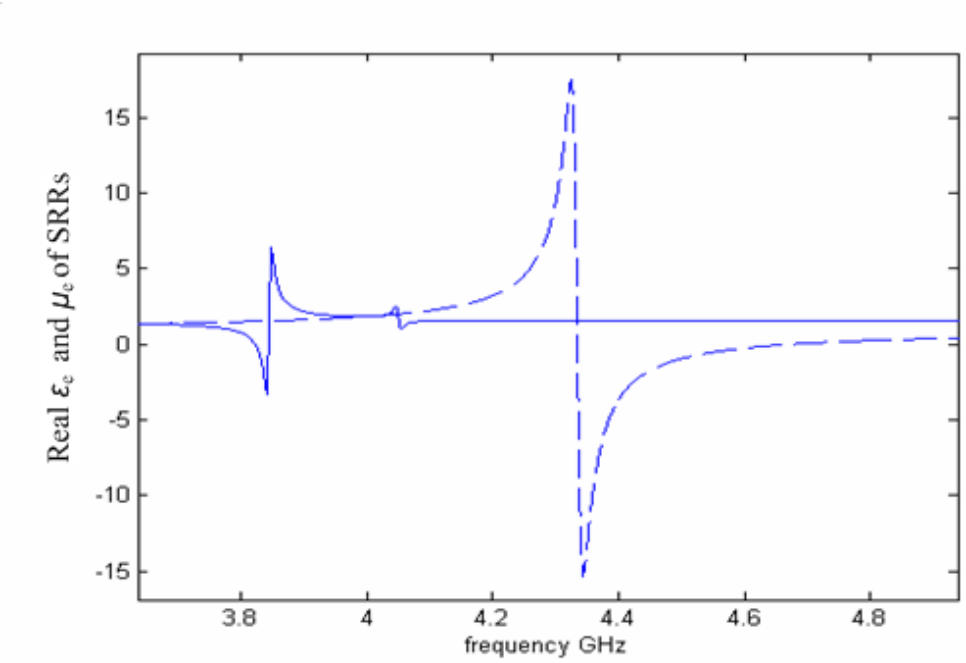

Figure 4-1: Real parts of electric permittivity (solid) and magnetic permeability (dashed) of the cubic SRR structure studied in Chapter 2

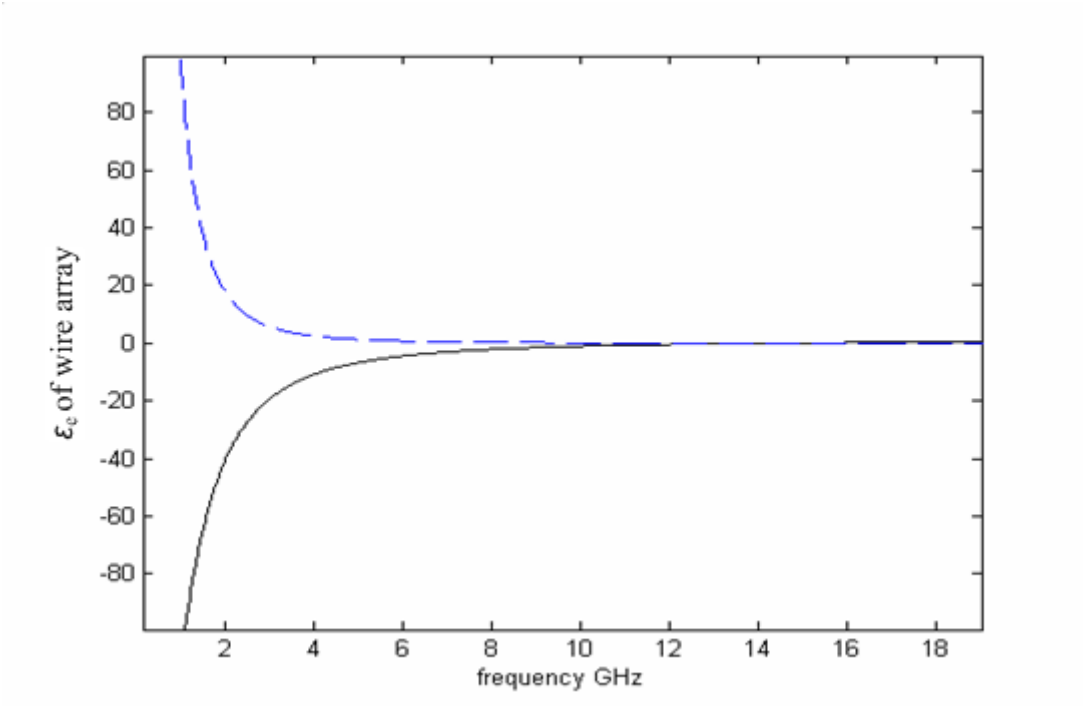

Figure 4-2: Effective permittivity of the aluminum wire array; real (solid) and imaginary (dashed) parts are plotted.

In Chapter 3, the metallic wire array is found to be nearly non-magnetic. (4.3) presents the effective permeability function for the reference structure. It may be clearly seen from (4.3) that the real part of the permeability tends to the unity since the lattice distance *a* should be chosen to be much greater than the wire radius *r* so that the effective medium theory stays valid and the Bragg diffraction effects can be eliminated.

$$\mu_{eff} = 1 - \frac{\pi r^2}{a^2}\left[1 + i\frac{2\sigma}{\omega r \mu_0}\right]^{-1} \tag{4.3}$$

Since $r<<a$, (4.3) may be reduced in a more compact form as (4.4)

$$\mu_{eff} \approx 1 + i\frac{\pi r^3 \omega \mu_0}{2\sigma a^2}, \qquad \sigma >> \omega r \mu_0 \tag{4.4}$$

Above analyses point out that the SRR structure and metallic wire array exhibit significant and novel electric and magnetic characteristics however, none of these structures alone has the capability to yield the desired left handed characteristics. In view of that fact, SRRs and metallic wires are composed in a way that the resulting structure would be able to possess double negative parameters. In Fig. 4-3, schematic presentation of the unit element for the composite metamaterial structure is given. However, there still exists the restriction that the periodicity of the unit cells should be arranged in a way that the lattice distance, the wire radius and SRR loop width are much smaller than the wavelength of the radiation. This condition is necessary to satisfy the condition of the effective medium theory as applied to this composite metamaterial structure.

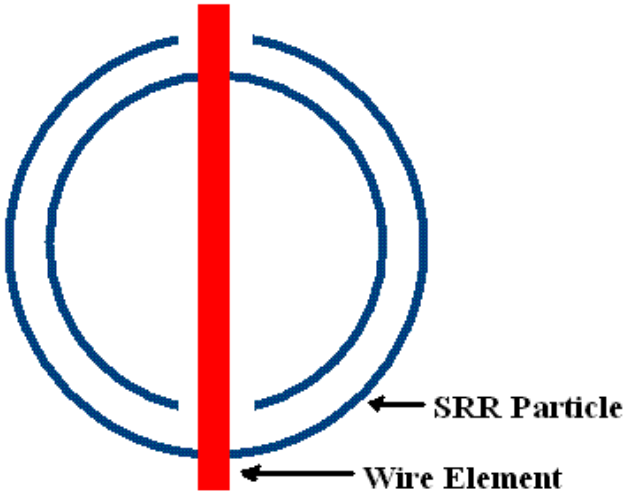

Figure 4-3: Composite SRR and Wire Element Structure

The real parts of the effective permittivities of the SRRs and wire array are shown in Fig 4-4, together. It may be seen from this figure that permittivity characteristic of the SRRs is quite weak compared to that of the wire array. Thus, the permittivity of the wire array dominates in the overall composite structure. In the other words, it is reasonable to deduce that the permittivity characteristic of the composite structure is mainly determined by the wire array.

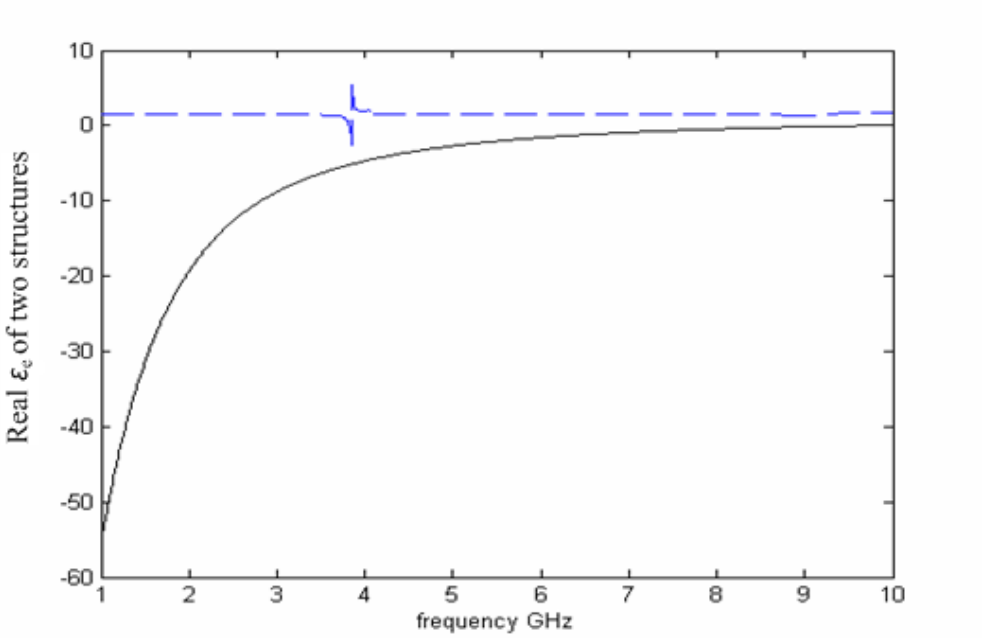

Figure 4-4: The real parts of effective permittivity functions of thin wire array (solid) and SRR cubic structure (dashed)

Similarly, for the permeability case, the real parts of the effective permeability functions of the SRRs and of the wire array are plotted in Fig. 4-5. As seen from this figure, the wire array produces almost no magnetic resonance. Thus, the permeability characteristic of the composite left handed structure is determined by that of the SRR elements, only.

Both the permittivity and the permeability investigations, covered so far, agree very well with the other observations in literature. Consequently, the permittivity characteristic of the wire array and the permeability characteristic of the SRRs could be accepted altogether as the negative medium parameter characteristics of the overall composite structure. Therefore, any variation in the relevant behaviors of the wire array and the SRRs will directly affect the overall response of the composite metamaterial structure. In view of that fact, the parameters affecting the responses of the wire array and of the SRRs are investigated in the next chapter.

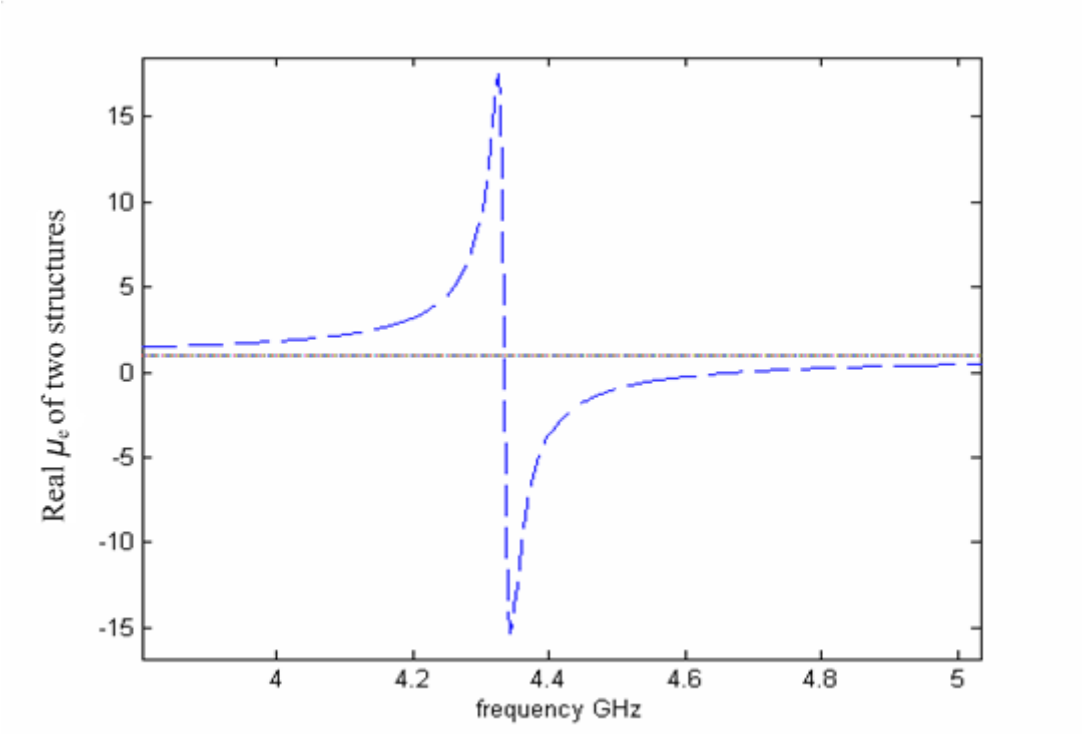

Figure 4-5: The real parts of effective permeability functions of thin wire array (solid) and SRR cubic structure (dashed)

CHAPTER 5

PARAMETERS AFFECTING THE RESONANCE BEHAVIOR OF METAMATERIALS

As discussed in the previous chapters, the metallic wires may be used to obtain negative permittivity and the SRR elements may be used to obtain negative permeability. Based on these results, a composite left handed metamaterial model is developed and its electromagnetic behavior is examined. The proposed composite model was basically a combination of the metallic wires and the SRR elements. Since two separate elements are used in the composite structure, each individual element is expected to have its own electric and magnetic behavior. Thus in the composite model, there will be a need to overlap the electromagnetic responses of the wire array and SRR structure and relevantly each structure should be designed to give the desired electric and magnetic response around the same frequency region. For this purpose, the parameters affecting the resonance responses of each element are going to be investigated in this chapter.

The electrical characteristics of the composite model are mostly determined by the metallic wires as discussed in Chapter 4. Furthermore, it is also seen that metallic wire array provides a very wide range of negative permittivity region under the plasma frequency. Thus, the negative permittivity region of the composite model may be altered by arranging the relevant plasma frequency of the wire array. Even though it seems quite flexible to arrange the negative permittivity region of the wire

array, in fact there exists the restriction of the wire and lattice sizes as discussed previously; the lattice distance and the wire radius should be much smaller than the wavelength of the radiation, i.e. a, $r << 2\pi C_o \omega^{-1}$. Considering this limitation, adjusting the plasma frequency (5.1) of the composite model becomes the main design criterion for the permittivity characteristics. It is worth to note that the SRR elements do not contribute to the permittivity behavior significantly since their electrical responses are quite negligible compared to the wires as observed in Chapter 4. Equation (5.1) gives the expression of the effective plasma frequency for an array of metallic wires. Here, n_{eff} is the effective density, m_{eff} is effective mass of the charge, r is the element radius and a is the lattice constant.

$$\omega_p^{\,2} = \frac{n_{eff} e^2}{\varepsilon_0 m_{eff}} = \frac{2\pi c_0^{\,2}}{a^2 \ln(a/r)} \tag{5.1}$$

On the contrary, the magnetic characteristics of the composite structure are observed to be determined by the SRR elements. Considering the analytical model derived for the permeability of SRR structures in Chapter 2, the permeability function is seen to be mostly dependent on the capacitive and inductive effects between the loops and the splits. Thus, tuning the permeability function is a bit more complicated than modifying the permittivity function.

In the following subsection the tuning possibilities of the SRR structure and the wire array are going to be investigated. Tuning the responses of these elements will alter the electromagnetic response of the overall composite model.

5.1 Changing the Resonance Frequency of the SRR Element:

A SRR element enhances its electromagnetic response mainly due to the mutual capacitive interactions between the two concentric rings and the capacitive effect between the splits of each ring [15]. Capacitance due to the splits prevents current from flowing around the rings but the mutual capacitance between the two rings

enables the flow of the current through the structure [3]. Thus the equivalent capacitance of the SRR element may be composed of mainly two parts; one arising from the splits and the other from the gap between the concentric rings. Inductances arise from the conducting rings and gap between inner and outer rings [7]. Then in order to change the resonance behavior of the SRR element, total impedance should be altered in a way that the desired resonance behavior is obtained. The effects of changing the SRR parameters are going to be investigated in the following sections, inspired from the works done in [15].

5.1.1. Effect of Split Width:

In this section, the effect of changing the split width on the permeability behavior of SRR elements is going to be investigated. During the investigation, the split width is altered while the rest of the parameters are kept constant. In this section, the analytical model derived in Chapter 2 will be used. There is a great difference between our analytical model structure used in Chapter 2 and the one studied in [15] Our analytical model was derived for a three dimensional cubic type of periodicity as presented in Fig 2-12 but the SRRs in [15] were oriented along periodic planes as shown in Fig. 5-1. Thus, the frequency region and the magnitude of the simulated resonance may vary compared to the results in [15].

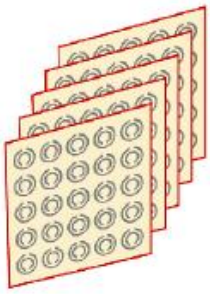

Figure 5-1: SRR element orientation in the structure suggested in [15]

In order to maintain coherence, the SRR parameters are taken as in Chapter-2. Accordingly, r_o is the strip radius, a_1, a_2 are the loop radii of outer and inner ring respectively, d is the spacing between the two loops and δ is the split spacing of both rings as presented in Fig. 2-5.

The values of the parameters are chosen to be the same as in [15]. Therefore $d = \delta = 0.2$ mm, $r_o = 0.45$ mm, $a_1 = 3.15$ mm, $a_2 = 2.05$ mm and the dielectric constant of the host medium $\varepsilon_r = 3.85$. The values of the split width δ are set to $\delta = 0.2$, 0.3, 0.4, 0.5 mm and the corresponding effective permeability values of the cubic structure of SRR elements are simulated by the analytic model derived in Chapter 2. The simulation results are presented in Fig. 5-2.

The simulated permeability functions indicate that the resonance frequency of the SRR structure increases by increasing the split width. Using the analytical model described in Chapter 2, the total capacitance of the structure is observed to decrease. This event could be described by assuming the splits as parallel plate capacitors where the capacitance decreases by increasing the distance between the plates. Since the capacitance due to splits decreases, the total capacitance also decreases, yielding an increase in the resonance frequency, ω_m.

Equation (5.2) presents the resonance frequency expression derived in Chapter 2 for such a structure. Variation of magnetic resonance frequency with split widths is given in Fig. 5-3. The resonance frequency is seen to increase by increasing the split width. The studies in [15] also predict same kind of resonance variation when the split width is increased. Hence, the simulation results obtained from the derived analytical model agree with the results reported in [15].

$$\omega_m^2 = \frac{1}{\sqrt{C_1 C_2 (L_1 L_2 - M^2)}} \tag{5.2}$$

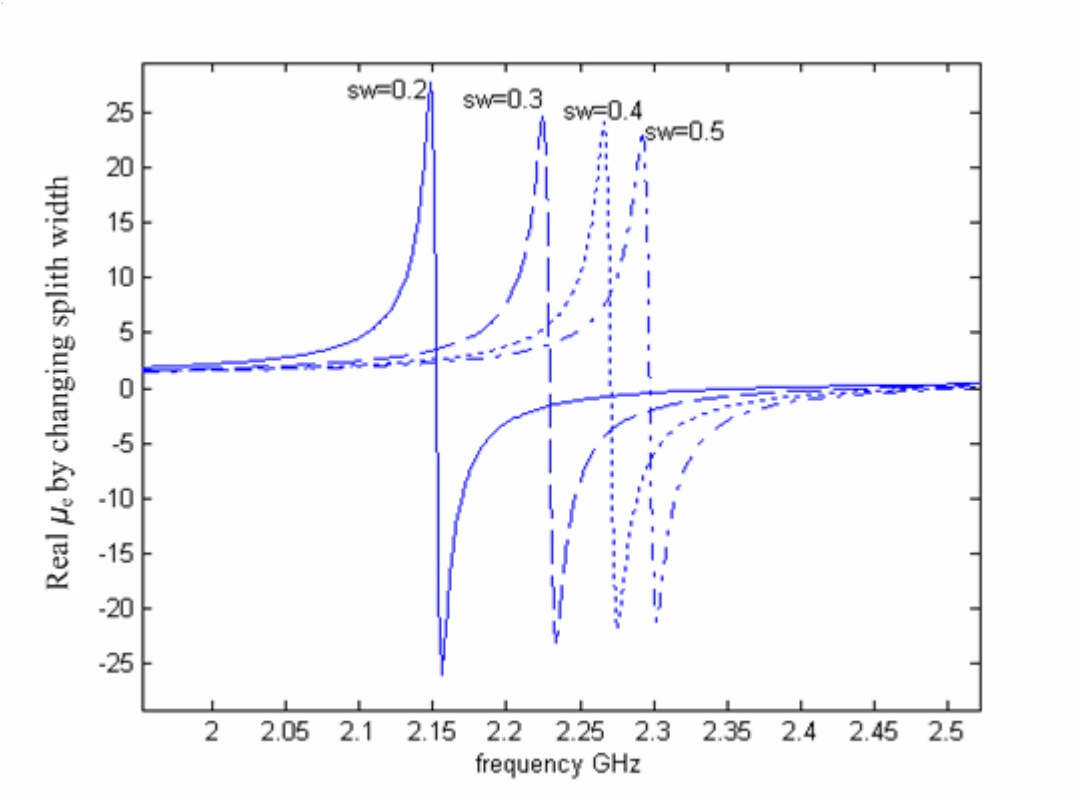

Figure 5-2: Real part of the magnetic permeability of the SRR array for different values of the split widths. Split widths are taken as 0.2 mm (solid), 0.3 mm (dashed), 0.4 mm (dot) and 0.5 mm (dashed-dot).

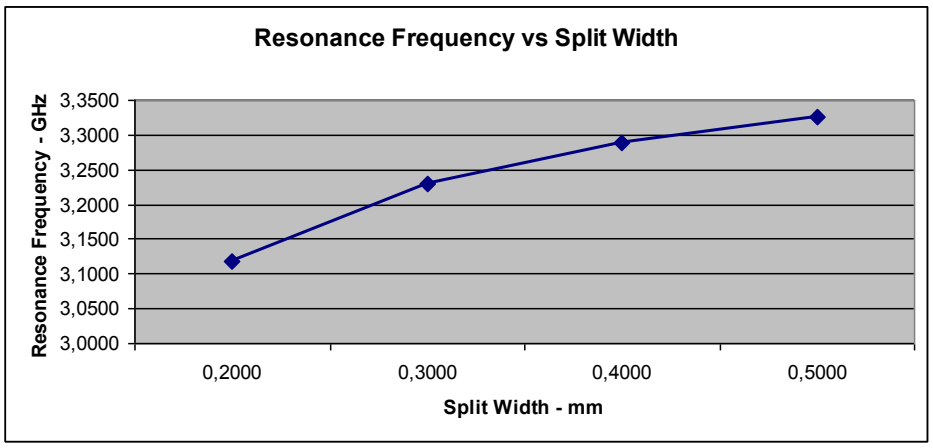

Figure 5-3: Variation in resonant frequency of SRRs due to changing split width

5.1.2. Effect of the Gap Distance:

In this section, the effect of changing the gap distance between the two rings of the SRRs on the permeability function is investigated. In doing so, the parameters other than the gap distance are kept constant at split width δ = 0.2 mm, wire radius r_o =0.45 mm, outer ring radius a_1 = 3.15 mm, inner ring radius a_2 = 2.05 mm and the dielectric constant of the host medium ε_r = 3.85. Then gradually the gap distance d is altered as d = 0.2 mm, 0.3 mm, 0.4 mm, 0.5 mm and the variation in magnetic permeability of the SRR structure is computed by a Matlab code. In the simulations, the analytical permeability function previously derived in Chapter 2 is used and the simulation results are presented in Fig 5 4.

The simulation results exhibit an increasing resonance frequency, ω_m, by incresing the gap distance between the two loops of SRRs. It is already studied in Chapter -2 that mainly two factors contribute to the total capacitance of SRRs, one is due to the split width in each loop and the other is due to the mutual interaction between the loops. Considering the analytical model, increasing the gap distance between the loops yields a decrease in the mutual capacitance term. Hence the total capacitance decreases and as discussed previously the resonance frequency, ω_m, increases. Variation of the resonance frequency by changing the gap distance is described in Fig 5-5.

5.1.3. Effect of the Ring Width:

For the purpose of investigating the effects of changing the strip radius, the other parameters are kept constant at $d = \delta$ = 0.2 mm, a_1 = 3.15 mm, a_2 = 2.05 mm and ε_r = 3.85. Then the strip radius is decreased as r_o = 0.45 mm, 0.35mm, 0.25mm and the variation in the resonant frequency is observed via simulating the analytical permeability function by a Matlab code. The results of the simulation are reported in Fig 5-6.

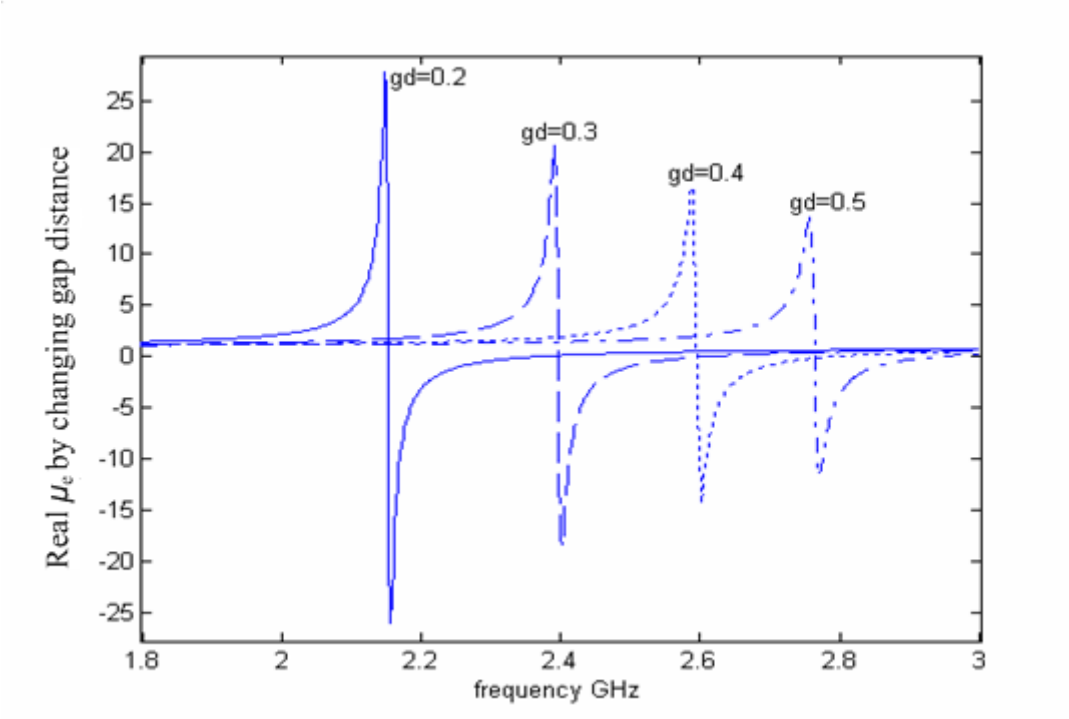

Figure 5-4: Real part of the magnetic permeability of SRR elements for different values of the gap distance. Gap distances are taken as 0.2 mm (solid), 0.3 mm (dashed), 0.4 mm (dot) and 0.5 mm (dashed-dot).

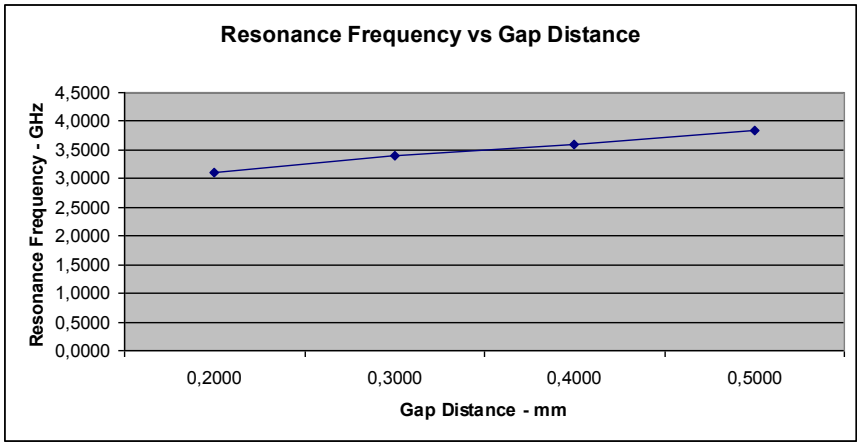

Figure 5-5: Variation in resonant frequency of SRRs due to changing gap distance

The simulation results indicate that increasing the ring width between the two loops of SRRs increases the magnetic resonance frequency. Regarding the analytical model, changing the ring width is observed to affect both the capacitances and inductances of the structure. However, considering the total effect, increasing the metal width results in decreasing total impedance. Thus, as in the previous sections, the resonance frequency increases by decreasing the total impedance. Consequently, SRRs made up of thinner rings will posses lower resonance frequencies [15].

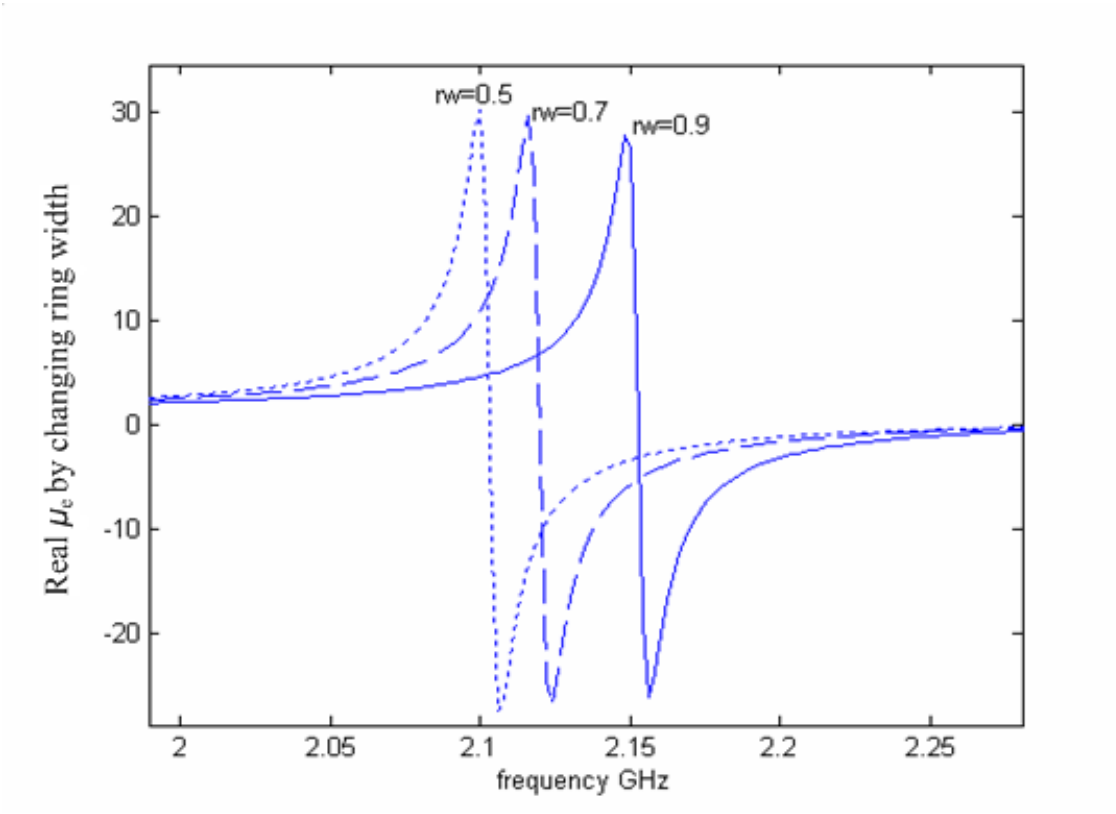

Figure 5-6: Real part of the magnetic permeability of SRR elements for different values of the ring widths. Ring widths are taken as 0.9 mm (solid), 0.7 mm (dashed), 0.5 mm (dot).

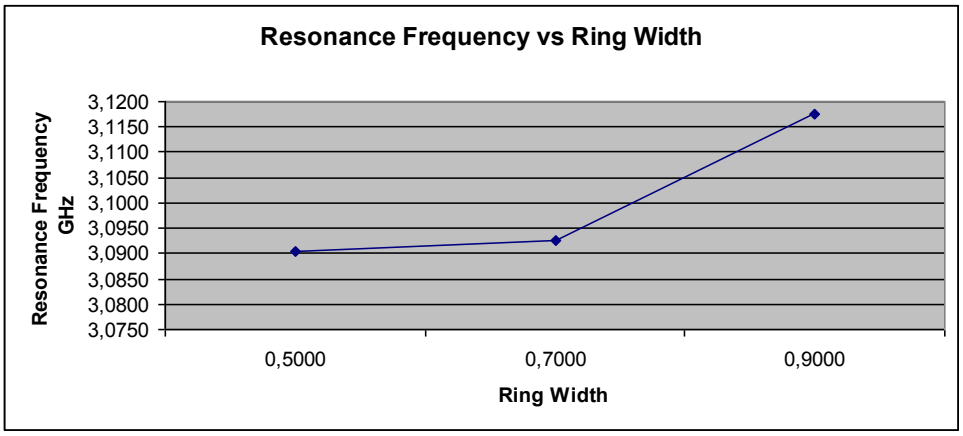

Figure 5-7: Variation in resonant frequency of SRRs due to changing ring width

5.1.4. Effect of the Additional Capacitance:

In view of the previous investigations, it is expected that every change in the total capacitance is going to affect the resonance behavior of SRR elements. Thus in this section, the effect of additional capacitance on the resonance frequency is going to be investigated. For this purpose, a capacitor is mounted in parallel to the outer ring's split and the value of the capacitor gradually altered from 0.1 pf to 0.8 pf. Similarly, rest of the parameters are kept the same at their reference values; $d = \delta =$ 0.2 mm, r_o =0.45 mm, a_1 = 3.15 mm, a_2 = 2.05 mm and the dielectric constant of the host medium ε_r = 3.85. The change in the resonance behavior is computed by a Matlab code with the results plotted in Fig. 5-8 based on the analytical model of Chapter 2.

In the previously reported studies, the role of the capacitance is indirectly examined since every change in the size parameters affected the total capacitance as well as the total impedance. Relevantly, the simulation results in Fig 5-8 agree with the previous studies in a way that the resonant frequency decreases by increasing the total capacitance. It is also worth to note that the change in the resonance frequency is quite abrupt in response to changes in the capacitance.

Considering the previous methods proposed to change the resonance frequency, there is an obligation to resize the SRR structure. If it is attempted to lower the resonance frequency as in Fig 5-8 without any additional capacitance, the overall structure needs to become larger. However, via adding a varactor to the splits, tuning the resonance band of the SRR structure could be maintained without any restriction of the resizing of the system. Hence the proposed method could be accepted as a significant approach in obtaining a tunable SRR structure. [15]

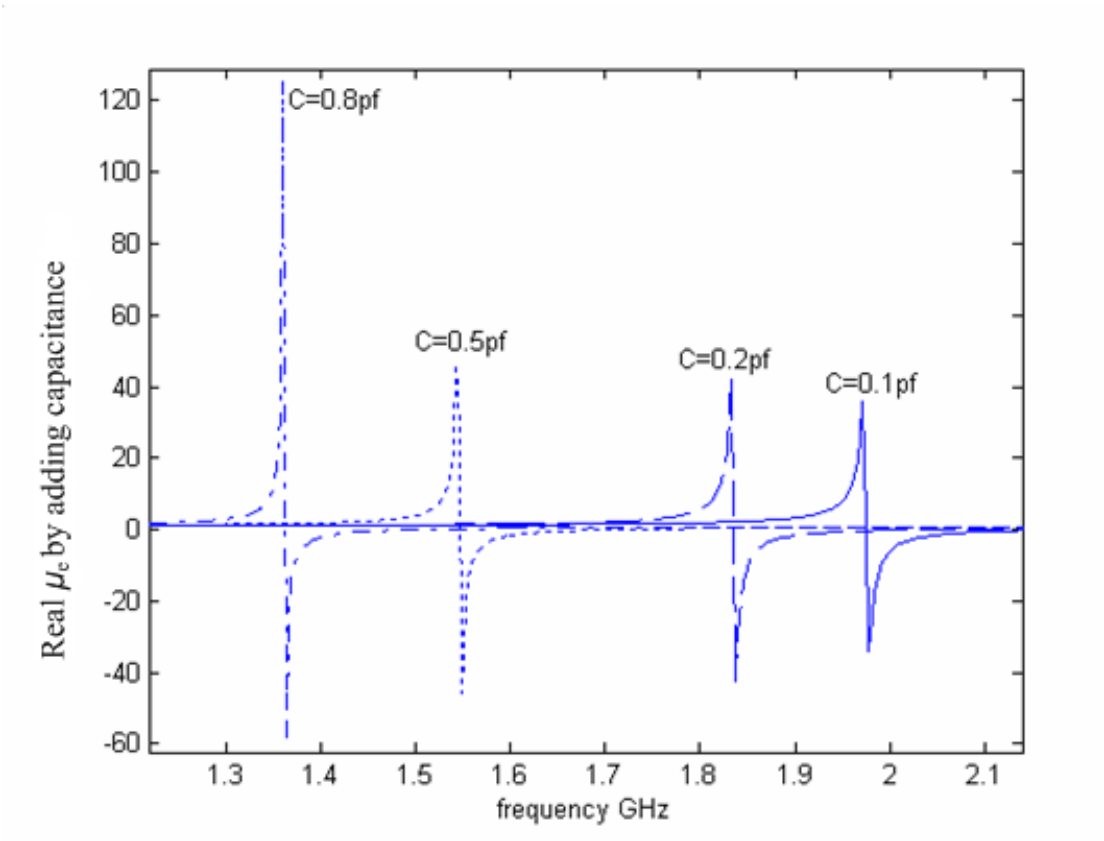

Figure 5-8: Real part of the magnetic permeability of SRR array for different values of the additional capacitance across the outer ring split. Capacitance values are taken as 0.1 pf (solid), 0.2 pf (dashed), 0.5 pf (dot) and 0.8 pf (dashed-dot).

5.1.5. Effect of the Substrate Permittivity:

Considering the analytical model of the effective permeability, the host medium is as well defined as a variant. The tuning capability of this parameter was not discussed in [15]. However, in this thesis, the role of this parameter is also investigated for tuning the SRR structures.

For the sake of coherence, the notations and the values are taken as $d = \delta = 0.2$ mm, $r_o = 0.45$ mm, $a_1 = 3.15$ mm and $a_2 = 2.05$ mm. Then, the medium relative permittivity of the medium is set to values of as 3.85, 2.85, and 1.85. Corresponding variations in the permeability function are computed and plotted in Fig 5-9.

The simulation results indicate that increasing the relative permittivity of the host medium yields a decreasing resonant frequency. Again considering the analytical model, the medium permittivity shows up as a numerator term in the mutual capacitance formula, thus decreasing the permittivity gives a decreasing mutual capacitance leading to a decrease in the total capacitance. The reported results show the importance of the host medium to modify the permeability of the composite metamaterial. If the permittivity of the host medium varies, the resonance of the overall structure can also be changed.

5.2 Changing the Resonance Frequency of the Wire Array:

The electrical characteristics of the composite left handed metamaterial is determined by the metallic wire array as mentioned previously. Thus, changing the effective permittivity of the metallic wire array must lead to changes in the effective permittivity of the composite structure. In this section tuning capabilities of the electric permittivity of the wire element array are going to be investigated.

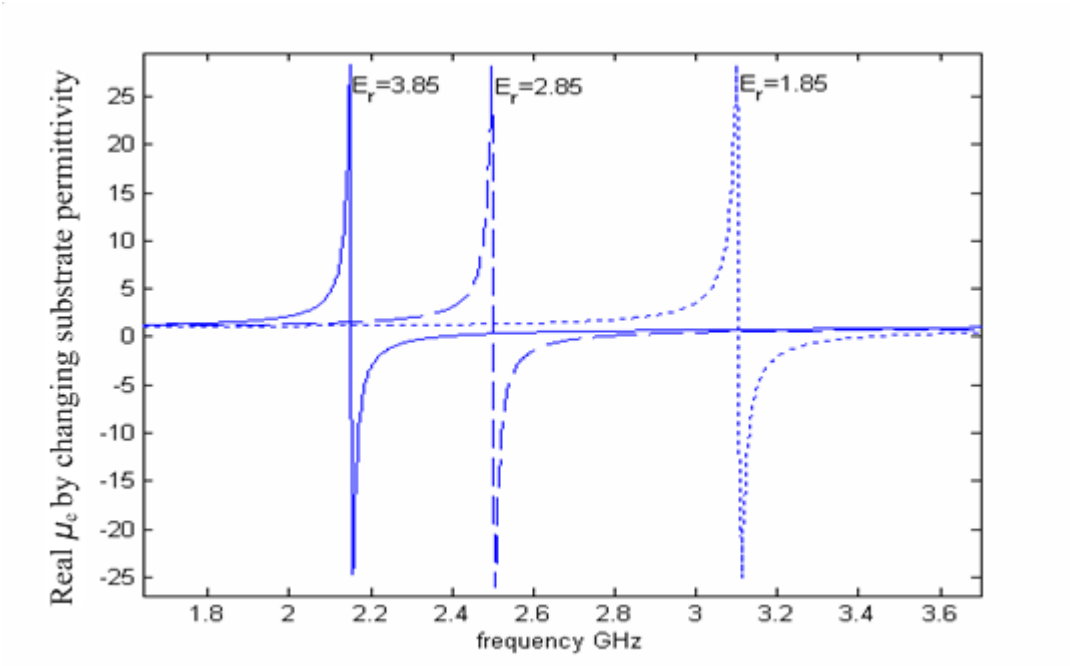

Figure 5-9: Real part of the magnetic permeability of SRR array for different values of the substrate relative permittivity. The permittivities are taken as 3.85 (solid), 2.85 (dashed), 1.85 (dot).

In fact, there are two key parameters affecting the effective permittivity response of the wire array; the radius *r* and the lattice distance *a*. Thus, the tuning investigations are done through changing these two parameters. Equation (5.3) describes the effective permittivity and equation (5.4) describes the plasma frequency of such arrays as derived in Chapter 3. However, it must be emphasized again that the radius and the lattice distance should be chosen much smaller than the wavelength of the radiation, i.e. $a, r << 2\pi C_o \omega^{-1}$ in order to meet the effective medium theory approximation and to minimize the Bragg refraction effects through the wire elements.

$$\varepsilon_{eff} = 1 - \frac{\omega_p^{\,2}}{\omega(\omega + i\varepsilon_0 a^2 \omega_p^{\,2} / \pi r^2 \sigma)} \tag{5.3}$$

$$\omega_p{}^2 = \frac{n_{eff} e^2}{\varepsilon_0 m_{eff}} = \frac{2\pi c_0{}^2}{a^2 \ln(a/r)} \tag{5.4}$$

5.2.1. Effect of the Wire Radius:

Again for the sake of coherence, the metallic wires are chosen to be made up of aluminum and the geometrical dimensions are taken as in Chapter-3. Therefore element radius r = 1.0 x 10^{-6} m and the lattice constant of a = 5.0 x 10^{-3} m are taken as reference values. Since the wires are chosen to be aluminum, the density of electrons in one aluminum wire is n = 1.806 x 10^{29} m^{-1}, yielding an effective mass of m_{eff} = 2.4808 x 10^{-26} kg as calculated in Chapter 3. In order to investigate the effect of the wire radius on the overall permittivity response, the wire radius is changed as r = 0.5, 1.0, 1.5, 2.0 x 10^{-6} m while the rest of the parameters are kept constant. The electric permittivity of the wire array is then computed by a Matlab code using the model derived in Chapter 3. The simulation results are presented in Fig. 5-10.

These results show that the plasma frequency decreases by decreasing the wire radius. This observation also agrees with the plasma frequency formula in (5.4). Increasing the radius of the wires may be a practical approach to increase the negative permittivity region. However, it should be noted that if the radius of the wires get larger, it would be comparable with the lattice distance then the Bragg diffraction effects become significant. Moreover, enlarging the wire radius will also violate the effective medium theory condition $a, r << 2\pi C_o \omega^{-1}$. Therefore, the capability of tuning the permittivity resonance via altering the wire radius could be applicable to certain extent.

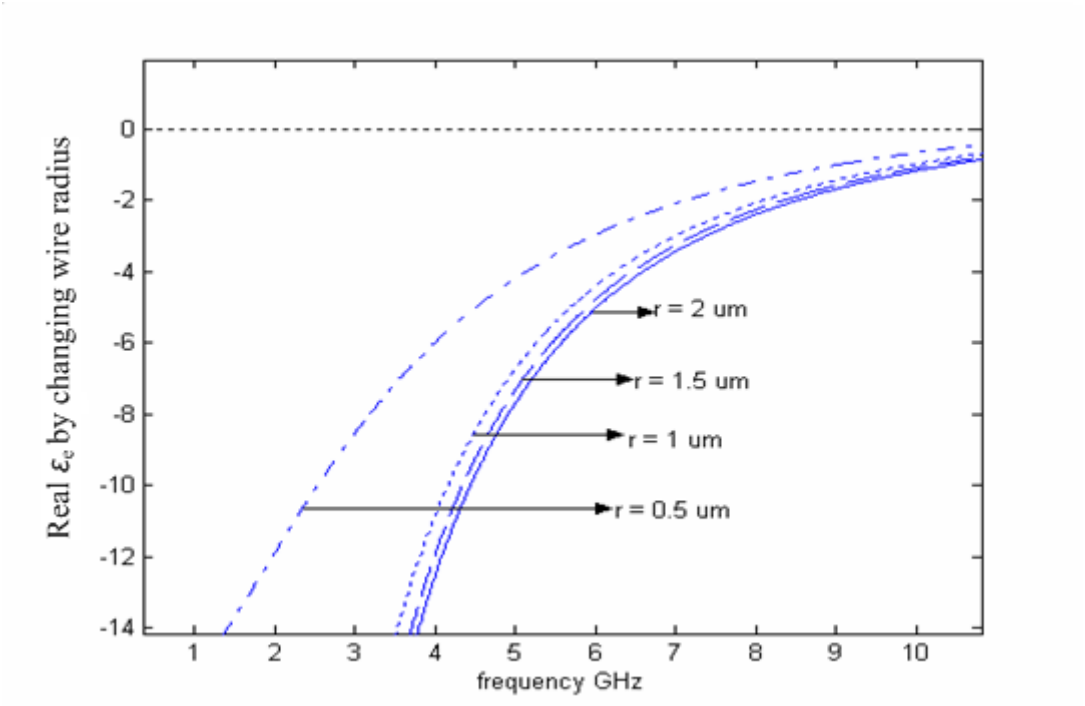

Figure 5-10: Real part of electric permittivity of the wire array for different values of the wire radius. The radii are taken as 0.5 μm (solid), 1.0 μm (dashed), 1.5 μm (dot) and 2.0 μm (dash-dot)

5.2.2. Effect of the Lattice Distance:

In this section, effects of the lattice distance on the permittivity function of the wire array are going to be investigated. Again the wires are chosen to be aluminum and the radius is kept constant, r = 1.0 x 10^{-6}, as in the reference model of Chapter 3. Then, the permittivity function is computed by a Matlab code as the lattice distance is increased as a = 5.0, 6.0, 7.0 x 10^{-3} m. The simulation results are presented in Fig. 5-11. As expected from (5.4), the plasma frequency is decreased by increasing the lattice constant since it shows up as a denominator term.

It may be seem quite effective to tune the wire array via altering the lattice distance between the wires while satisfying the key restriction $a, r << 2\pi C_o \omega^{-1}$ not to violate the condition of the effective medium approximation.

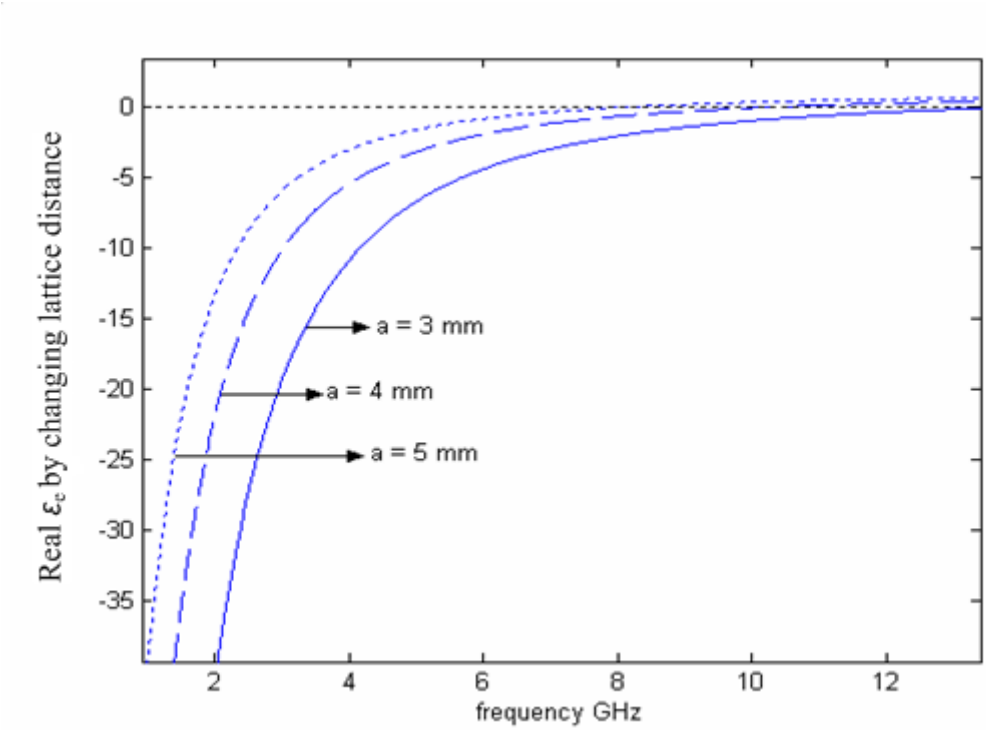

Figure 5-11: Real part of the effective permittivity of the wire array for different values of the lattice distance. The lattice distances are taken as 3 mm (solid), 4 mm (dashed), 5 mm (dot)

CHAPTER 6

CONCLUSION

Permittivity and permeability parameters are known to determine the electric and magnetic characteristics of a given medium. For naturally occurring materials, these parameters take positive values. However for a left handed metamaterial, permittivity and permeability are desired to be double negative. The reversal of the signs of these parameters affects several parameters of the relevant medium and gives rise to innovative applications. Because of these reasons, left handed metamaterials attract significant attention and numerous studies are devoted to this subject. In this thesis, such materials are theoretically investigated through the topics of obtaining negative permeability and negative permittivity together with the resonance frequency tuning possibilities.

Since there exists no natural material having simultaneous negative permittivity and negative permeability characteristics, a left handed metamaterial had to be developed artificially. In doing so, each one of the negative parameters are obtained using a separate artificial structure; the negative permittivity may be provided by a metallic wire array and negative permeability is provided by Split Ring Resonators. Consequently, the left handed metamaterial is built via composing the wire array and the SRRs.

In this thesis, obtaining negative permeability issue is investigated in Chapter 2. Since natural materials do not exhibit negative permeability property, an artificial

structure named Split Ring Resonator (SRR) was developed and reported in literature. The analytical permittivity and permeability formulas for the SRR structure are also studied and simulated by relevant Matlab codes. Simulation results indicated that SRR structure is capable of giving negative permeability response. However, the electrical resonance of the SRR structure is weaker than its magnetic resonance. Moreover, the electrical and magnetic resonance regions of the SRR are observed not to overlap. As a result, to obtain the negative permittivity characteristics, another structure is needed.

For obtaining the negative permittivity values, the metallic wire array is used in literature since it is capable to simulate the plasma medium . Plasma is known to produce negative permittivity response below the plasma frequency but this frequency is seen at much higher frequencies than the microwave band. Thus, the first concern was reducing the plasma frequency. It is seen than by sufficiently thin metallic wires, the plasma frequency may be reduced to the microwave range. Then, an analytical formula for the permittivity and the permeability of a wire array can be developed. Such formulas are computed by proper Matlab codes in this thesis. The simulations indicated that the wire array presents a very wide negative permittivity region with almost zero magnetic response.

Considering the results of the studies concerning SRRs and metallic wire array, it is seen that none of these artificial structures alone are capable to exhibit the desired double negative parameters. Thus, these structures are combined in a way that the composite structure would be able to indicate the left handed material characteristics. The permittivity characteristic of the composite structure is determined by the wire elements and the permeability characteristic is determined by the SRR elements.

After obtaining the left handed metamaterial structure, parameters affecting the permittivity and permeability responses are studied as well . In doing so, the SRR structure and the wire elements are investigated separately. The investigations are

done by using the analytical models obtained previously for the relevant permittivity and permeability functions. For the SRR structure, the permeability characteristics are altered via changing the total capacitive effect. For the wire array, there are two main design parameters, the lattice distance and the wire radius. Both for the SRRs and the wire array, the variations in the effective medium parameters are investigated through simulations. Additionally, resonance frequency tuning in the composite left handed structure have been examined by changing the structural parameters of the SRR and wire arrays, changing them one at a time.

To conclude, in this thesis, the theory behind the metamaterial structures of SRRs and thin wire arrays are studied in detail based on the reported researches in literature. Results of the modeling studies are simulated using Matlab codes written in this thesis work. Additionally, the effects of changing the structural parameters of the SRR and thin wire arrays on the resonance frequency, effective permeability and effective permittivity of the composite double negative metamaterial structure are investigated through simulations. The simulation results obtained in this work are found in very good agreement with the results repeated in literature.

Future work in this area may focus on the theoretical investigation of alternative metamaterial structure other than the well known SRRs with periodic wire arrays.

.

REFERENCES

[1] V. G. Veselago, "The electrodynamics of substances with simultaneously negative values of permittivity and permeability," *Sov. Phys. USPEKHI,* vol. 10, p. 509, 1968.

[2] J. B. Pendry, A. J. Holden, W. J. Stewart and I. Youngs, "Extremely Low Frequency Plasmons in Metallic Mesostructures," *Phys. Rev. Lett*., vol. 76, p. 4773, 1996.

[3] J. B. Pendry, A. J. Holden, D. J. Robbins, and W. J. Stewart, "Low frequency plasmons in thin-wire structures," *Journal of Physics: Condensed Matter*, vol. 10, p. 4785, 1998.

[4] J. B. Pendry, A. J. Holden, D. J. Robbins, and W. J. Stewart, "Magnetism from conductors and enhanced nonlinear phenomena," *IEEE Trans. Microwave Theory Tech.*, vol. 47, p. 2075, 1999.

[5] D. R. Smith, Willie J. Padilla, D. C. Vier, S. C. Nemat-Nasser, and S. Schultz, "Composite medium with simultaneously negative permeability and permittivity" *Phys. Rev. Lett*. vol. 84, p. 4184, 2000.

[6] W. Rotman, "Plasma simulation by artificial dielectrics and parallel plate media," *IRE Trans. Antennas. Propagat*., vol. 10, pp. 82–95, 1962.

[7] C. R. Simovski, B. Sauviac and S. A. Tretyakov "Double Split-Ring Resonators: Analytical Modeling and Numerical Simulations", *Electromagnetics*, 24:317–338, 2004.

[8] Qun Wu, Fan-Yi Meng, and Ming-Feng Wu, "Research on the Negative Permittivity Effect of the Thin Wires Array in Left-Handed Material by Transmission Line Theory", *Progress In Electromagnetics Research Symposium*, p. 196, 2005.

[9] Marques, R., F. Medina, and R. Rafii-El-Edrissi. 2002. Role of bianisotropy in negative permeability and left-handed metamaterials. *Phys. Rev. B* 65:1440/1-440/6.

[10] Lagarkov, A. N., V. N. Semenenko, V. A. Chistyaev, D. E. Ryabov, S. A. Tretyakov, and C. R. Simovski. 1997. Resonance properties of bi-helix media at microwaves. *Electromagnetics* 17:213–237.

[11] Tretyakov, S. A., F. Mariotte, C. R. Simovski, T. G. Kharina, and J.-P. Héliot. 1996. Analytical antenna model for chiral scatterers: Comparison with numerical and experimental data. *IEEE Transactions on Antennas and Propagation* 44:1006–1014.

[12] Antenna Handbook: Theory, Applications and Design, Y.T. Lo and S.W. Lee, Eds., NY: *Van Nostrand Reinhold*, 1988, ch. 7.

[13] F. Mariotte, S.A. Tretyakov, B. Sauviac, Modeling effective properties of chiral composites, *IEEE Antennas Prop. Mag*, Vol. 38, No. 2, pp. 22-32, 1996.

[14] Caloz, C. and Itoh T., "Application of the Transmission Line Theory of Left-Handed (LH) Materials to the Realization of a Microstrip 'LH line'," *IEEE Antennas and Propagation Society International Symposium*, 412-415, 2002.

[15] Koray Aydin, Irfan Bulu, Kaan Guven, Maria Kafesaki, Costas M Soukoulis and Ekmel Ozbay, "Investigation of magnetic resonances for different split-ring resonator parameters and designs", *New Journal of Physics 7*, 168, 2005.

[16] R.W.P. King, The loop antenna for transmission and reception, in *Antenna theory Part1*, R.E. Collin and F.J. Zucker, Eds., NY, McGraw Hill, 1969.

[17] J. D. Jackson, *Classical Electrodynamics*, John Wiley and Sons, NY, 1962.

[18] R.A. Shelby, D.R. Smith, and S. Schultz, "Experimental Verification of a negative Index of Refraction," *Science*, vol. 292, pp. 77–79, April 2001.

[19] R. F. Whitmer, "Principles of microwave interactions with ionized media; Part I: Plasma resonance," *Microwave J.*, vol. 2, pp. 17-19; February, 1959.

[20] Philippe Gay-Balmaz and Olivier J. F. Martin, "Electromagnetic resonances in individual and coupled split-ring resonators", *J. Appl. Phys.*, vol. 92, no. 5, 2002.

[21] D. R Smith, W. Padilla, D. C. Vier, S. C. Nemat-Nasser, S. Schultz, "Negative Permeability from Split Ring Resonator Arrays", *IEEE JSTuA5*, 2000.

[22] Yi-Jang Hsu, Yen-Chun Huang, Jiann-Shing Lih, and Jyh-Long Chern, "Electromagnetic resonance in deformed split ring resonators of left-handed meta-materials", *J. Appl. Phys.*, vol. 96, pp. 1979, 2004.

[23] M. F. Khan , M. J. Mughal, "Effective permeability of inner ring shorted split ring resonator", *Microwave and Opt. Tech. Let.*, vol. 50, pp. 624 – 627.